author copy; published version: https://doi.org/10.1021/acssynbio.9b00108

Streamlined *Pseudomonas taiwanensis* VLB120 chassis strains with improved bioprocess features

Benedikt Wynands[1,2], Maike Otto[1,2], Nadine Runge[1], Sarah Preckel[1], Tino Polen[1], Lars M. Blank[1], and Nick Wierckx[1,2]*

1. Institute of Applied Microbiology, RWTH Aachen University, Worringerweg 1, 52074 Aachen, Germany
2. Institute of Bio- and Geosciences, IBG-1: Biotechnology, Forschungszentrum Jülich GmbH, 52425 Jülich, Germany

*: corresponding author,
Nick Wierckx, Institute of Bio- and Geosciences, IBG-1: Biotechnology, Forschungszentrum Jülich GmbH, 52425 Jülich, Germany, e-mail: n.wierckx@fz-juelich.de, phone: +49 2461 61 85247

Abstract

Microbes harbor many traits that are dispensable or even unfavorable under industrial and laboratory settings. The elimination of such traits could improve the host's efficiency, genetic stability, and robustness, thereby increasing the predictability and boosting its performance as a microbial cell factory.

We engineered solvent-tolerant *Pseudomonas taiwanensis* VLB120 to yield streamlined chassis strains with higher growth rates and biomass yields, enhanced solvent tolerance, and improved process performance. In total, the genome was reduced by up to 10%. This was achieved by the elimination of genes which enable the cell to swim and form biofilm and the deletion of the megaplasmid pSTY and large proviral segments. The resulting strain GRC1 had a 15% higher growth rate and biomass yield than the wildtype. However, this strain lacks the pSTY-encoded efflux pump TtgGHI, rendering it solvent-sensitive. Through re-integration of *ttgGHI* by chromosomal insertion without (GRC2) and with (GRC3) the corresponding regulator genes, the solvent-tolerant phenotype was enhanced. The generated *P. taiwanensis* GRC strains enlarge the repertoire of streamlined chassis with enhanced key performance indicators, making them attractive hosts for biotechnological applications. The different solvent tolerance levels of GRC1, GRC2, and GRC3 enable the selection of a fitting host platform in relation to the desired process requirements in a chassis *à la carte* principle. This was demonstrated in a metabolic engineering approach for the production of phenol from glycerol. The streamlined producer GRC1Δ5-TPL38 outperformed the equivalent non-streamlined producer VLB120Δ5-TPL38 concerning phenol titer, rate, and yield, thereby highlighting the added value of the streamlined chassis.

Graphical abstract:

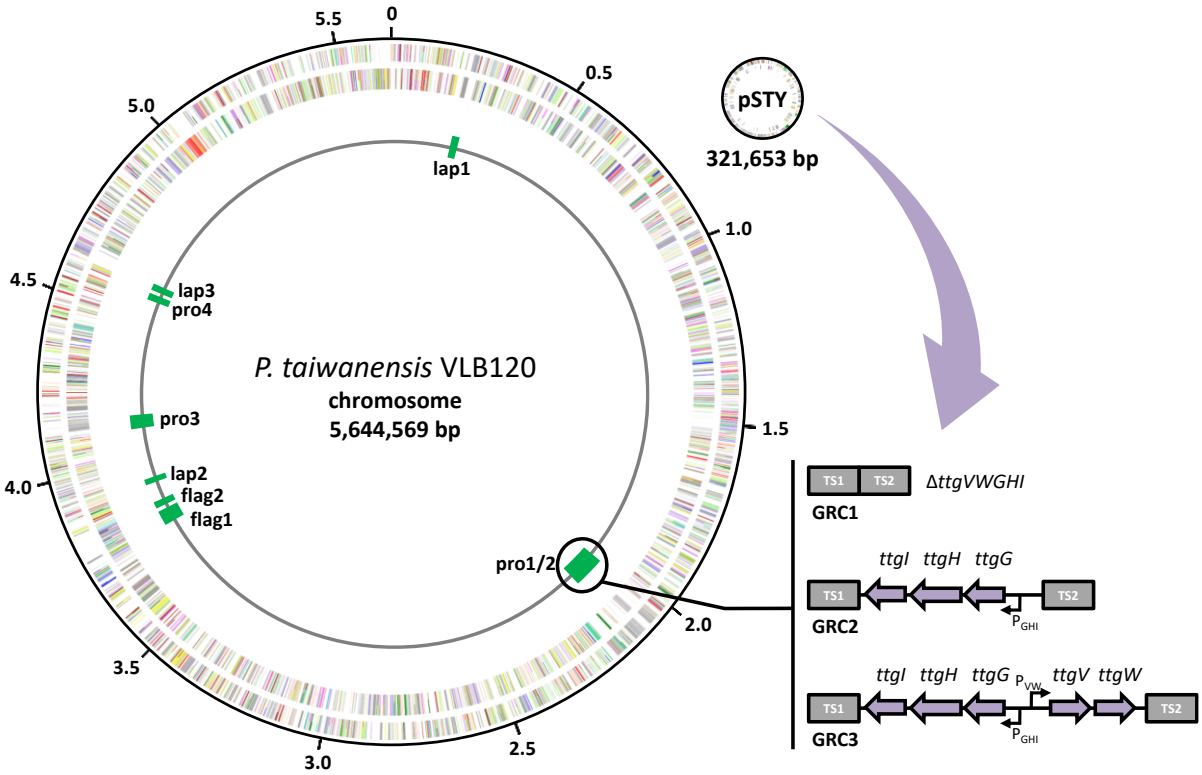

Schematic overview of the *P. taiwanensis* VLB120 wildtype genome with the chromosomal position of the target regions (green) and the megaplasmid pSTY that were deleted to obtain streamlined chassis strains. The proviral segment pro1/2 was deleted (strain GRC1) or replaced by the efflux pump encoding genes *ttgGHI* without and with the regulatory genes *ttgVW* in strain GRC2 and GRC3, respectively. The outer ring of colored bars indicates the plus strand, the inner the minus strand. The individual colored bars represent genes located at the respective loci of the two DNA strands according to their clusters of orthologous groups (COGs) classification.

Keywords:
Streamlined chassis; Genome reduction; Solvent tolerance; *Pseudomonas*; Metabolic engineering; Phenol

1. Introduction

Synthetic biology has empowered us to rationally engineer microbial catalysts to synthesize a wide range of valuable organic chemicals from renewable resources in eco-friendly biological processes[1]. However, the potential of microbial cell factories has not been exploited to its full degree yet and a large proportion of current research focuses on expanding their industrial applicability by improving key bioprocess performance indicators such as titer, rate, and yield, as well as substrate and product tolerance.

Besides metabolic engineering, which certainly is a key strategy to improve product formation through specific flux alterations of existing and/or integration of novel pathways[2], microorganisms can also be tailored addressing general cell functions to enhance their overall fitness and performance in biotechnological processes[3]. Microbes have evolved under the selective pressure of their natural surroundings, which are far removed from the anthropogenic biotechnological environment. Hence, they harbor many traits that might play important roles in their ecological niches, but are dispensable or even unfavorable for laboratory and industrial settings[4]. Yet, nature provides solutions to ecological challenges that might also appear during biochemical synthesis processes such as tolerance mechanisms to cope with substrate or product toxicity[5-7]. The gain of knowledge and the advancing availability of new synthetic biology tools for precise and rapid DNA recombination allow a domestication of microbes of academic and industrial relevance by implementation of desired features and/or by targeted clearance of unfavorable characteristics[8-10]. Which characteristics exactly are desirable and dispensable should be defined according to the process conditions and objectives, as some features might be critical for certain processes but unfavorable for others[4]. Thus, the microbial host should ideally be chosen from a repertoire of different chassis strains according to a chassis *à la carte* principle[11].

In the past, multiple streamlined chassis strains of industrially relevant bacteria such as *Escherichia coli*[12,13], *Bacillus subtilis*[14,15], *Corynebacterium glutamicum*[16], *Pseudomonas putida*[17], and *Pseudomonas chlororaphis*[18] were generated. Superfluous cell functions were eliminated by targeted (large-scale) deletions, yielding genome-reduced chassis strains that showed enhanced characteristics compared to their progenitors. Among others, the major benefits were an increased genetic stability[13,19], an enhanced fitness under stress-triggering conditions[20,21], increased growth rates and biomass yields[22], and a boosted heterologous gene expression[17,20,22,23]. Additionally, the genome-reduced *E. coli* strain MDS42 was used as a platform for a following metabolic engineering approach, yielding an L-threonine producing biocatalyst that outperformed its wildtype-based reference strain harboring the same metabolic modifications with a 1.83-fold increased production, presumably resulting from a relief of metabolic burden[24]. The use of genome-reduced *Pseudomonas chlororaphis* strains yielded an increased production of phenazines[18]. These examples impressively demonstrated that the use of custom-tailored chassis strains can be a valuable contribution for an efficient production of industrially relevant products.

In this study, we focused on expanding the applicability of *Pseudomonas* for laboratory and industrial biotechnology through the generation of genome-reduced chassis strains of the solvent-tolerant *P. taiwanensis* VLB120[25]. Pseudomonads have been used for the production of a multitude of different organic chemicals including aromatics, rhamnolipids, terpenoids, polyketides, and prodiginines[26-28]. One key feature is their outstanding tolerance towards organic solvents such as *n*-octanol and toluene, which is not only beneficial for the production of such toxic compounds, but also allows a wider degree of freedom in the synergistic application of solvent extraction for *in situ* product removal[29,30].

For *P. putida* KT2440, it was already shown that the targeted deletion of dispensable cell components has a high potential for the generation of enhanced cell factories[17,22]. The elimination of flagella, prophages, transposons, and DNA restriction modification systems yielded strain EM383, a chassis with a 4.3% reduced genome. This strain showed higher biomass yield coefficients, an increased energy charge and reducing power, as well as an enhanced heterologous gene expression compared to the wildtype. Additionally, EM383 had an increased fitness under SOS response-triggering conditions and tolerance towards oxidative stress[17,22]. However, *P. putida* KT2440 lacks one of the major solvent resistance pumps that are the main determinants of solvent tolerance. Therefore, we focused on the chassis engineering of the solvent-tolerant *P. taiwanensis* VLB120. This bacterium features several promising characteristics for industrial applications. It was isolated from forest soil as styrene degrader and extensively studied for its (*S*)-styrene oxide producing capacity[25,31,32]. Additionally, it has been used for the bioproduction of isobutyric acid, (*S*)-3-hydroxyisobutyric acid, isobutanol, *n*-octanol, and phenol[33-35]. *P. taiwanensis* VLB120 possesses a unique solvent tolerance and can grow in the presence

of a second phase of aliphatic alcohols and hydrophobic aromatics. In contrast to other solvent-tolerant Pseudomonads, *P. taiwanensis* VLB120 is non-pathogenic and inherently capable of assimilating D-xylose[36].

By targeted elimination of the pSTY megaplasmid, large proviral segments, flagella- and biofilm-associated gene clusters, we reduced the genome of *P. taiwanensis* VLB120 by ~10% and obtained tailored chassis strains with improved characteristics including higher growth rates and biomass yields. The ability to swim and form biofilm was eradicated, as these functions are needless or unfavorable in most laboratory settings. By chromosomal re-integration of the pSTY-encoded efflux pump genes *ttgGHI*, with and without its transcriptional regulators, the solvent tolerance was engineered to yield the constitutively and inducibly tolerant *P. taiwanensis* strain GRC2 and GRC3, respectively. Along with the solvent-sensitive GRC1, these strains enable a selection of solvent tolerance levels that can be tailored to the envisioned product and process, while also sporting enhanced key performance indicators such as reduced biofilm formation, increased growth rate, and biomass yield. The superior performance of the GRC strains was exploited in a metabolic engineering approach aiming for a more resource-efficient synthesis of phenol from glycerol. The streamlined producer GRC1Δ5-TPL38 showed enhnaced production parameters regarding phenol titer, rate, and yield compared to the equivalent non-streamlined producer VLB120Δ5-TPL38.

2. Results and Discussion

2.1. Elimination of swimming capability by the deletion of large flagellar clusters

2.1.1. Genetic analysis

Flagella are widespread among bacteria. The ability to actively move and respond tactically to chemical gradients or physical stimuli can increase the fitness of environmental bacteria, justifying the metabolically costly synthesis of the flagellar machinery and its energy-intense operation[37,38]. However, for their use in laboratory and industrial setups the microbe's ability to swim is usually dispensable because the culture broth is usually well-mixed. Under these circumstances, the synthesis and rotation of flagella pose needless sinks of metabolic resources and energy[39].

Inspired by the work of Martinez-Garcia et al.[39] on strain *P. putida* EM329 (= KT2440Δflagella), we decided to construct a flagella-less variant of the solvent-tolerant bacterium *P. taiwanensis* VLB120. The flagellar cluster of this strain is similar to that of *P. putida* KT2440 and they both harbor an interstitial segment encoding flagella-unrelated enzymes and hypothetical proteins. Yet, the genetic context of this segment as well as the number and function of the encoded proteins differ, although both contain genes related to cell wall biosynthesis. Instead of eliminating the whole flagellar cluster including this segment in a single deletion procedure, we decided on consecutive deletions of two regions denoted as flag1 and flag2 (Table 1), leaving the interregional segment intact. This was done to reduce the risk of undesired side effects, as some of the observed phenotypes of *P. putida* EM329 might be the result of the deletion of flagella-unrelated genes[39].

Table 1 The genetic segments deleted within this study are listed with a description, their position according to accession number CP003961.1, the number of coding sequences (CDS), their size, and the relative proportion of the total genome size.

Name	Description	Position (bp)	Number of CDS	Size (kb)	Proportion of total genome (%)
pSTY	megaplasmid	extrachromosomal replicon	365	321.7	5.39
pro1/2	prophage 1/2	2025574-2131212	162	105.6	1.77
pro3	prophage 3	4115506-4161797	61	46.3	0.78
pro4	prophage 4	4568696-4581079	17	12.4	0.21
pro5	prophage 5	5268120-5310003	52	41.9	0.70
flag1	flagellar genes	3767793-3812598	45	44.8	0.75
flag2	flagellar genes	3832716-3849243	18	16.5	0.28
lap1	biofilm-associated genes	204010-223295	6	19.3	0.32
lap2	biofilm-associated genes	3918406-3933516	7	15.1	0.25
lap3	biofilm-associated genes	4601770-4618483	5	16.7	0.28

All deletions were generated using the I-SceI-based system that allows scarless DNA clearance without an antibiotic resistance marker remaining in the genome[40]. The Δflag1Δflag2 double mutant was denoted as VLB120Δflagella. Additionally, strains only lacking either the flag1 or the flag2 region were generated. A detailed overview of the flagellar cluster, the flagella-unrelated DNA segment, and the deleted regions is given in the supplemental information (Table S1).

Multiple previous studies reported a relation between the disruption of flagella-related genes and solvent tolerance in *P. putida*. Yet, the results for highly solvent-tolerant strains such as S12 and DOT-T1E were quite different to those in the solvent-sensitive KT2440. Transcriptomic studies revealed that multiple genes involved in flagella synthesis were repressed in KT2440 when exposed to toluene while there was no transcriptional change concerning these genes in DOT-T1E[41,42]. Volkers et al.[43] even reported a transcriptional up-regulation of flagellar genes in the presence of toluene for *P. putida* S12. Thus, it is surprising that inactivation of several flagellar genes caused solvent sensitivity towards *n*-octanol and toluene in *P. putida* S12 and *P. putida* DOT-T1E, respectively[44,45]. However, a non-motile yet solvent-tolerant strain of DOT-T1E was obtained by a *fliL*::Ω-Km gene disruption[45]. Since the solvent tolerance of *P. taiwanensis* VLB120 is a unique feature that we did not want to compromise, we additionally constructed VLB120Δ*fliL* (ΔPVLB_17160) as control strain for following solvent tolerance tests. FliL is a flagellar body-associated protein. Orthologues of this protein can be found in almost every swimming bacterial species, yet its sequence is not very conserved[46] and its function has not been fully understood yet[47,48]. Furthermore, its deletion in different bacterial genera has led to diverse phenotypes[46].

2.1.2. Evaluation of swimming capability

To study the effect of the aforedescribed deletions, VLB120 (wildtype), VLB120Δ*fliL*, VLB120Δflag1, VLB120Δflag2, and VLB120Δflagella were characterized concerning their swimming capability on mineral salt medium (MSM) plates containing 20 mM glucose and 0.3% (w/v) agar (Figure 1).

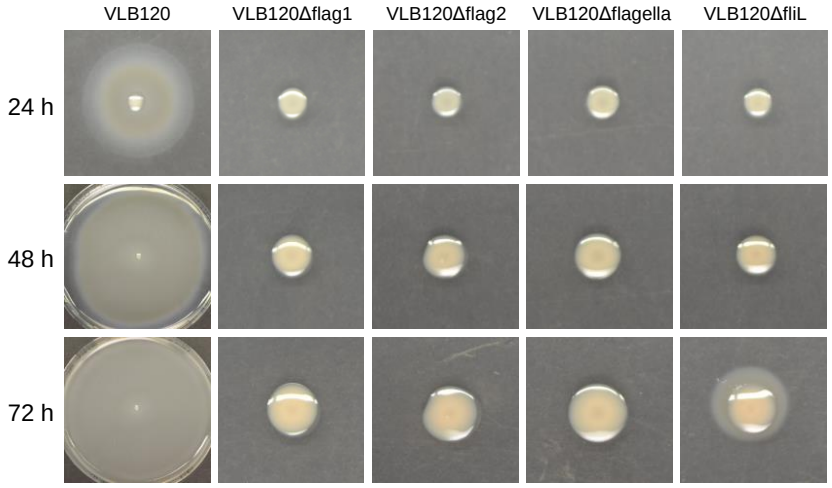

Figure 1. The swimming capability of VLB120 (wildtype), VLB120Δ*fliL*, VLB120Δflag1, VLB120Δflag2, and VLB120Δflagella was assessed on a mineral salt medium (MSM) plate containing 20 mM glucose and 0.3% (w/v) agar. Cell suspensions were spotted onto the plates. Pictures were taken after 24, 48, and 72 h of incubation at 30°C. The grown bacterial spots are true to scale and thus comparable amongst themselves concerning their size, with the exception of the pictures shown for the wildtype after 24 and 48 h.

For the wildtype, a distinct halo surrounding the initial spot can be observed after 24 h, demonstrating the reference strain's ability to swim. With prolonged incubation time, this halo continuously spread radially until it reached the Petri dish wall as seen after 72 h. There was no detectable swimming behavior for all flagellar mutants after 24 and 48 h, although the Δ*fliL* mutant showed a small swimming halo after 72 h. VLB120Δflag1 and VLB120Δflag2 each only partially lack the large flagellar cluster. Both regions, flag1 and flag2, encode important flagellar genes that are involved in regulation and synthesis of flagella or directly encode structural flagellar proteins (Table S1). Thus, it is not surprising that both mutants showed no swimming capability.

For the non-flagellated strain *P. putida* KT2440 derivative EM329 an improved tolerance towards oxidative stress, an elevated adenylate energy charge, an increased reducing power[39], and a boosted

heterologous gene expression was reported[22]. Due to the close relation of *P. putida* and *P. taiwanensis* and the high similarity between the deleted flagellar clusters of these species it is very likely that VLB120Δflagella shares the same attributes, although they were not investigated within this study.

2.2. Reducing biofilm formation by deletion of adhesive proteins

In addition to the above-stated benefits of the flagella-less *P. putida* variant EM329, an increased surface adherence was reported after prolonged cultivation[39]. The removal of the flagella could be directly responsible for an accumulation of sessile cells since they are essential for cell dispersion from biofilms to re-enter the planktonic life form[49].

To assess if the deletion of the flagella had a comparable effect in *P. taiwanensis* VLB120, the biofilm formation of VLB120Δflagella was quantified according to O'Toole[50] and compared to the wildtype. Therefore, the strains were statically grown in polyvinyl chloride 96 well "U" bottom plates with mineral salt medium containing 20 mM glucose. After an incubation time of 10 h, sessile cells were stained with crystal violet and photometrically quantified (Figure 2).

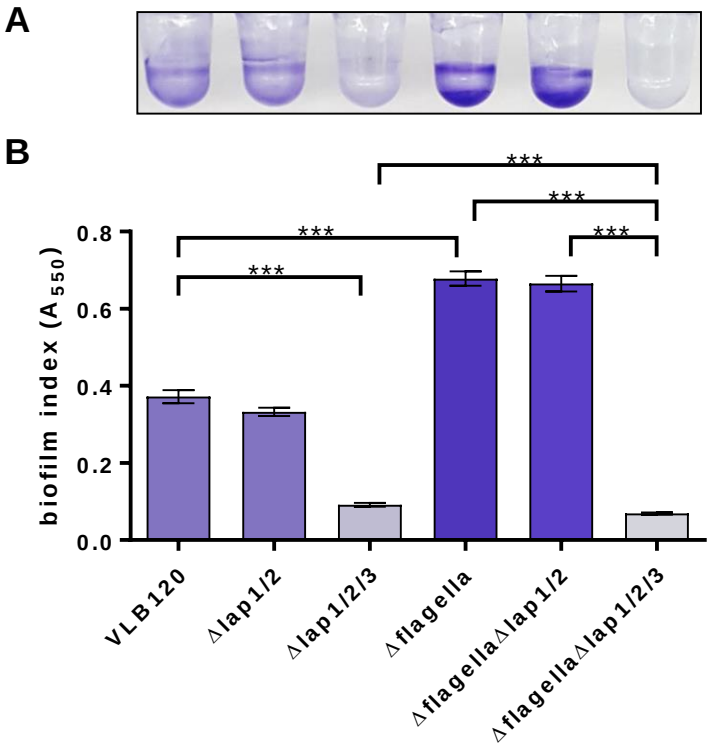

Figure. 2. The biofilm formation of flagellar and large adhesion protein mutants of *P. taiwanensis* VLB120 on the surface of polyvinyl chloride microtiter plates was examined after static incubation for 10 h in mineral salt medium containing 20 mM glucose. A side view picture of crystal violet stained biofilms of representative cultures (A) and the photometrically quantified biofilms as A_{550} are shown (B). The assay was performed in eight biological replicates. Error bars indicate the standard error of the mean (n = 8). Triple asterisks (***) indicate significance with *p*-values ≤ 0.002.

Crystal violet staining of the biofilm revealed that VLB120Δflagella indeed had a 1.8-fold higher tendency to form biofilm than the wildtype (Figure 2). Especially in the area of the well bottom increased adherent biomass was visible for this strain. This is likely due to an increased sedimentation of VLB120Δflagella caused by the non-swimming phenotype[39]. In niche applications, surface-adherent bacteria can be beneficial for biotechnological applications as biofilms provide a protective environment against stressing agents[46,51,52]. In fact, biocatalytic biofilms of *P. taiwanensis* VLB120 were used for a robust bioproduction of (*S*)-styrene oxide and perillic acid from styrene and limonene, respectively[7,53,54], and the deletion of the flagellar clusters could be useful in such biofilm biocatalysis. In nature, biofilms are the predominant lifestyle of bacteria[55], but in most laboratory and industrial settings planktonic cells are commonly preferred over sessile cells. Therefore, we aimed to reduce biofilm formation. In *P. putida* KT2440, the large adhesive proteins (Lap) play a fundamental role in surface attachment and formation of microcolonies. LapA is required for the initial adhesion of single cells to biotic and abiotic surfaces, while LapF is involved in the later stages of biofilm formation mediating cell-cell interactions[56].

Previous studies on *P. fluorescens* and *P. putida* demonstrated that the inactivation of LapA alone led to a biofilm formation deficiency[57,58].

Genomic analysis of *P. taiwanensis* VLB120 revealed the presence of three large *lap* clusters (Table 1). The segment containing *lapA*, *lapB*, *lapC*, *lapD*, *lapG*, and one hypothetical gene was denoted as lap1 region. A second *lap* cluster *inter alia* comprised of *lapE* and genes encoding proteins showing homology to LapA, LapB, and LapC, was named lap2. The third segment encodes *lapF*, *lapH*, *lapI*, *lapJ*, and the chemotaxis protein-encoding gene *chev-1* and was denoted as lap3 region. A detailed overview of these *lap*-related regions and their genes can be found in the supplemental information (Table S2).

The lap1, lap2, and lap3 regions were successively deleted in the wildtype and VLB120Δflagella, yielding the strains VLB120Δlap1/2/3 and VLB120ΔflagellaΔlap1/2/3. These strains and their respective immediate progenitor strain still possessing the lap3 cluster (VLB120Δlap1/2 and VLB120ΔflagellaΔlap1/2) were tested for their biofilm-developing attributes. Surprisingly, the combined deletions of the *lapA*-encoding region lap1 and region lap2 had no significant effect on biofilm formation in both the wildtype and Δflagella background, although it had been previously reported that the inactivation of LapA lead to a loss of biofilm development in other Pseudomonads[57,58]. Possibly, the decision to eliminate the whole clusters including regulatory elements rather than exclusively the adhesin-encoding genes was responsible for these observations. For *P. putida*, a high cyclic di-GMP (c-di-GMP) level was reported to stimulate *lapA* expression while having a repressing effect on *lapF*[56]. The lap1 region encodes the diguanylate cyclase LapD. Its deletion could have led to a decrease in the intracellular concentration of c-di-GMP, possibly leading to an increased expression of LapF. Although it is reported that LapA is essential for biofilm initiation and LapF only contributes to later stages of biofilm development in *P. putida* KT2440[56], the additional deletion of the *lapF*-including lap3 region in *P. taiwanensis* VLB120 strains caused a dramatic decrease in biofilm, indicating that the roles of LapA and LapF could potentially overlap. The biofilm formed by VLB120Δlap1/2/3 (A_{550} = 0.09 ± 0.00) was 4.1-fold lower compared to the wildtype (Figure 2). VLB120ΔflagellaΔlap1/2/3 also showed a highly reduced biofilm formation (A_{550} = 0.07 ± 0.00) with a 9.7-fold decrease when compared to its progenitor VLB120Δflagella (Figure 2). Thus, the combinatory deletion of all three *lap* clusters led to the desired reduction of biofilm in the wildtype and VLB120Δflagella background.

2.3. Solvent tolerance and loss of the pSTY megaplasmid

The unique solvent tolerance of *P. taiwanensis* VLB120 is a key feature we wanted to retain. The elimination of the flagellar apparatus and large cell surface proteins such as LapA and LapF certainly influence the characteristics of the cell envelope. The flagella and LapF are known to be hydrophobic. Therefore, their removal is expected to increase the cell's hydrophilicity[39,59]. This in return can affect solvent tolerance due to changing interaction of the cell surface to hydrophobic solvents[59]. Additionally, the deletion of flagella and *lap* clusters could cause unforeseen effects, which alter solvent tolerance due to regulatory or physiological crosstalk. As already discussed in Section 2.1.1, a connection between flagella and solvent tolerance was reported in different solvent-tolerant *P. putida* strains, where inactivation of flagellar-associated genes led to solvent sensitivity in strain S12 and DOT-T1E[44,45]. Moreover, it was reported that the deletion of LapF elevated tolerance towards lipophilic *n*-octanol but decreased tolerance towards hydrophilic methanol in *P. putida* KT2440[59]. For this reason, we investigated the effects of the deletions of the flagellar apparatus and biofilm-associated adhesins on the solvent tolerance phenotype.

Solvent extrusion is the most crucial factor conveying solvent tolerance[60] and is primarily mediated by the TtgGHI efflux pump in *P. taiwanensis* VLB120[61]. In order to have an adequate negative control that is solvent-sensitive, the TtgGHI-coding megaplasmid pSTY (321.653 kb) was eliminated from the wildtype using a modified version of the I-SceI-mediated method with only one TS sequence, yielding strain VLB120ΔpSTY. In addition to TtgGHI efflux pump-encoding genes, the megaplasmid also carries genes that convey mercury resistance and styrene catabolism. The loss of the megaplasmid was verified by colony PCR, sensitivity towards 5 mg L^{-1} mercury chloride (Figure 3B), and the inability to use styrene as sole carbon source (Figure S1).

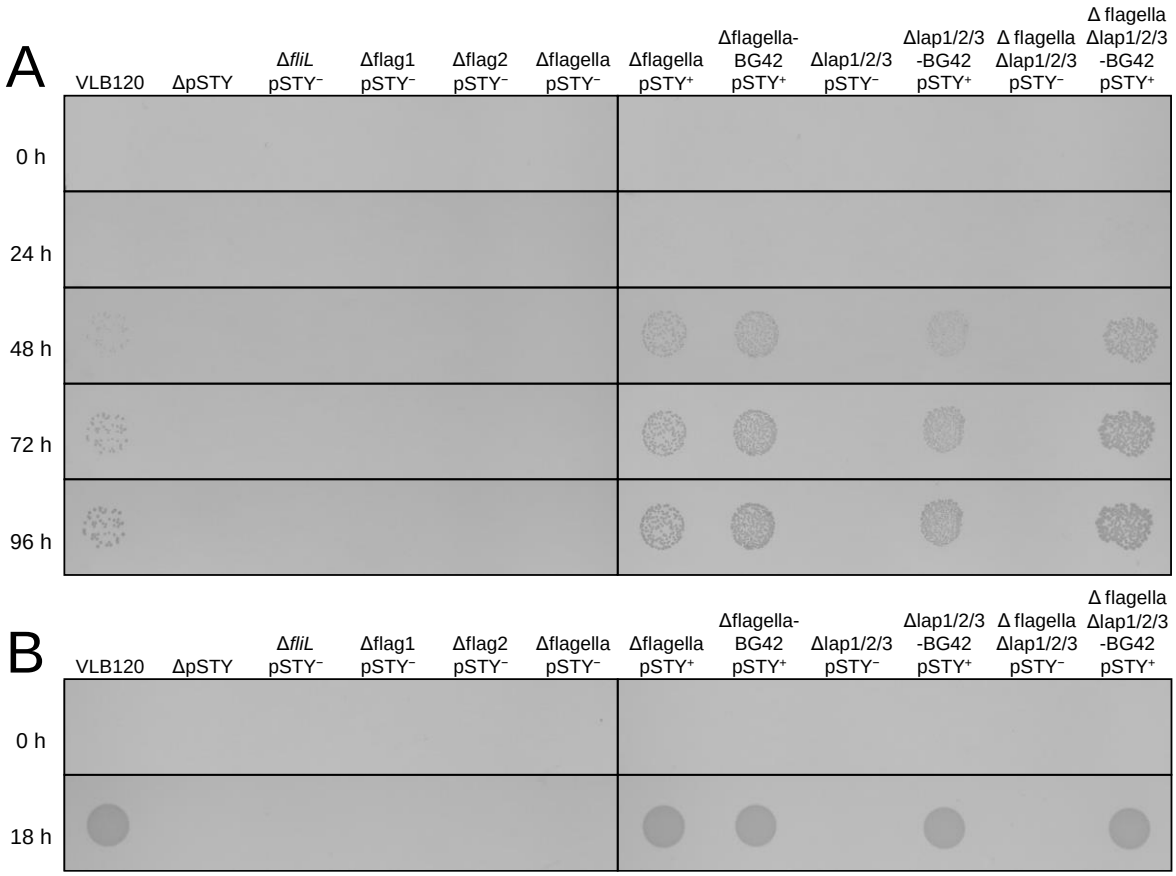

Figure 3. Growth of *P. taiwanensis* VLB120 (wildtype), VLB120Δ*fliL* pSTY$^-$, VLB120Δflag1 pSTY$^-$, VLB120Δflag2 pSTY$^-$, VLB120Δflagella pSTY$^-$, VLB120Δflagella pSTY$^+$, VLB120Δflagella-BG42 pSTY$^+$, VLB120Δlap1/2/3 pSTY$^-$, VLB120Δlap1/2/3-BG42 pSTY$^+$, VLB120ΔflagellaΔlap1/2/3 pSTY$^-$, and VLB120ΔflagellaΔlap1/2/3-BG42 pSTY$^+$ on LB agar plates exposed to styrene vapor for 6 h and subsequently covered with 70 mL of liquid toluene at room temperature (A). Growth of the same strains on LB plates containing 5 mg L^{-1} mercury chloride at 30°C (B). A cell suspension volume of 10 µL with an OD_{600} of ~0.01 was spotted. One representative dataset of three replicates is shown.

The generated strains were tested for their resistance towards toluene in an LB plate-based assay. Therefore, cell suspensions of the respective strains were spotted on an LB plate and grown for 6 h at room temperature in saturated styrene vapor to allow an initial adaptation before toluene was poured onto the plate. Growth was evaluated after subsequent incubation at room temperature. The results of this experiment are shown in Figure 3A. The wildtype showed visible colony formation after 48 h, indicating that at least a proportion of the initially spotted cells tolerated the 2nd layer of toluene and were able to grow. Previously, it has been demonstrated that VLB120 is able to grow under a layer of styrene under similar condition[31]. Expectedly, the VLB120ΔpSTY control strain failed to grow due to the absence of the TtgGHI efflux pump. However, the complete lack of growth for all the deletion strains VLB120Δ*fliL*, VLB120Δflag1, VLB120Δflag2, VLB120Δflagella, VLB120Δlap1/2/3, and VLB120ΔflagellaΔlap1/2/3 was rather surprising and the question arose if another fundamental phenomenon caused the severe loss of solvent tolerance. Therefore, these strains were tested for the possession of the megaplasmid pSTY by means of colony PCR using primers binding to *ttgH* and *ttgI*, mercury resistance, and styrene catabolism. Interestingly, colony PCR failed to give a positive result for VLB120Δflag1, VLB120Δflag2, VLB120Δflagella, VLB120Δlap1/2/3, and VLB120ΔflagellaΔlap1/2/3, while yielding the expected DNA fragment for the wildtype (data not shown). Additionally, all mutants failed to assimilate styrene (as exemplified for VLB120Δflagella pSTY$^-$ in Figure S1, supplemental information) and they could not grow in the presence of 5 mg L^{-1} mercury chloride (Figure 3B) in contrast to the wildtype. These results are a clear indication that the pSTY megaplasmid was lost in all four independent mutant lines generated within this study (Δ*fliL*, Δflag1, Δflag2, Δlap1). This phenomenon was reported in a previous study for an additional *P. taiwanensis* VLB120 mutant line (VLB120Δ5)[35], indicating that the loss of pSTY in engineered VLB120 strains is not an uncommon event. Yet, the wildtype strain stably maintains pSTY without the addition of a selecting pressure and such a frequent loss of the megaplasmid has not been reported

previously for other Pseudomonads. Further investigations indicated that the loss of pSTY is not related to the applied deletion methodology *per sé* as the pSTY loss appeared also upon conjugational transfer of other plasmids (data not shown). However, the phenomenon is not unique to mating procedures as it also appeared during electroporation of *P. taiwanensis* VLB120 (L. Schäfer, A. Schmid, UFZ Leipzig, personal communication).

The loss of the megaplasmid did not allow an evaluation of the influence on solvent tolerance caused by the chromosomal deletions because the pSTY loss caused the simultaneous forfeiture of TtgGHI and hence toluene tolerance. Therefore, we reconstructed the VLB120Δflagella mutant under pSTY-selective conditions granted by the addition of 5 mg L^{-1} mercury chloride to the Cetrimide agar plate used for cointegrate selection. The repetitive deletion procedure of individual DNA segments is a time-consuming process. To optimize deletion procedures in a time-wise manner, we aimed for the simultaneous deletion of the flag1 and flag2 region as a proof-of-principle. Therefore, we successively integrated the two deletion delivery plasmids, pEMG-flag1 mediating kanamycin resistance and pSEVA512S-flag2 mediating tetracycline resistance, into the genome. By a single subsequent conjugational delivery of pSW-2 we obtained the VLB120Δflagella $pSTY^+$ (= Δflag1Δflag2) double mutant. We re-introduced the pSTY megaplasmid by conjugation according to Ramos-Gonzalez et al.[62] into the other deletion strains by endowing them with a gentamicin resistance marker containing mini-Tn7 transposon obtained using the pBG42 plasmid constructed by Zobel et al.[63]. This allows the selection of recipients from the wildtype donor without affecting growth of the cell[63]. The re-integration of pSTY was verified by PCR (data not shown), mercury resistance (Figure 3B), and growth on styrene (data not shown).

In contrast to their respective $pSTY^-$ progenitors, VLB120Δflagella-BG42 $pSTY^+$, VLB120Δlap1/2/3-BG42 $pSTY^+$, and VLB120ΔflagellaΔlap1/2/3-BG42 $pSTY^+$ tolerated an overlay of toluene (Figure 3A), indicating that none of these genetic modifications led to an impairment of solvent tolerance. In fact, none of the $pSTY^+$ strains performed worse than the wildtype. However, this plate-based assay is only semi-quantitative as pictures were only taken daily. Nevertheless, one can conclude that neither the deletion of the flagella nor the elimination of the biofilm-associated adhesins resulted in a solvent sensitivity in *P. taiwanensis* VLB120. In case of flagella, this is in discordance with previous reports made for *P. putida* DOT-T1E and S12[44,45], which might in some cases be explained by the fact that in these studies the observed phenotype could also have been caused by a loss of the megaplasmid.

2.4. Growth kinetics in minimal medium with glucose

To investigate the impact of aforedescribed large-scale deletions (ΔpSTY, Δflag1/2, Δlap1/2/3) on the growth kinetics, selected strains were grown in MSM with 20 mM glucose as sole carbon source. Biomass formation was monitored either manually by sampling and OD_{600} measuring (Figure 4A), or non-invasively using the cell growth quantifier (CGQ) that measures the backscattered light (Figure 4B). In case of the latter, the initial OD_{600} and final cell dry weight (CDW) were measured offline, and the biomass yield was determined after 20 h of incubation to allow the conversion of scattered light to CDW and obtain the strains' biomass yield coefficients (Table 2). Growth rates were calculated form the manually sampled cultures because they give more reliable data in the early exponential phase when biomass concentrations are low[64] (Table 2).

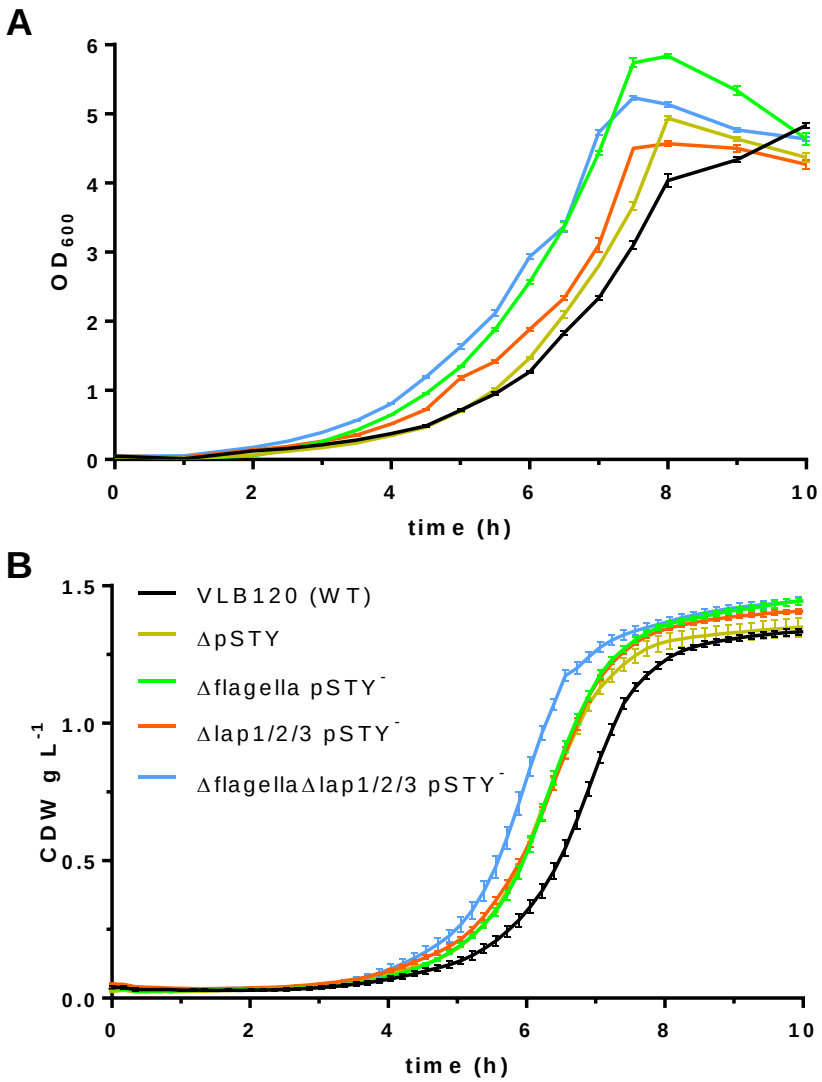

Figure 4. Growth of *P. taiwanensis* VLB120 (wildtype), VLB120ΔpSTY, VLB120Δflagella pSTY⁻, VLB120Δlap1/2/3 pSTY⁻, and VLB120ΔflagellaΔlap1/2/3 pSTY⁻ in shake flasks supplemented with MSM with 20 mM glucose obtained by manual sampling with offline measurement of the OD_{600} (A) and using the Cell Growth Quantifier (CGQ) with online scattered light measurement converted into CDW using end point biomass yields obtained for the respective cultures (B). Error bars indicate the standard error of the mean (n ≥ 3).

Table 2. Growth rates and biomass yield coefficients of selected deletion strains. The strains were grown in shake flasks on mineral salt medium (MSM) supplemented with 20 mM glucose. The errors are given as standard error of the mean (n = 3).

***P. taiwanensis* VLB120 strain**	**Growth rate μ (h^{-1})**	**Biomass yield coefficient $Y_{X/S}$ ($g_{cdw}\ g_{glucose}^{-1}$)**
wildtype	0.625 ± 0.003	0.372 ± 0.003
ΔpSTY	0.721 ± 0.028	0.377 ± 0.010
Δ*fliL* pSTY⁻	n.d.	0.395 ± 0.005
Δflag1 pSTY⁻	n.d.	0.421 ± 0.003
Δflag2 pSTY⁻	n.d.	0.402 ± 0.001
Δflagella pSTY⁻	0.837 ± 0.010	0.427 ± 0.004
Δlap1/2 pSTY⁻	n.d.	0.380 ± 0.006
Δlap1/2/3 pSTY⁻	0.707 ± 0.001	0.395 ± 0.003
ΔflagellaΔlap1/2/3 pSTY⁻	0.729 ± 0.007	0.424 ± 0.002
GRC1	0.721 ± 0.009	0.435 ± 0.002
GRC2	0.651 ± 0.009	0.396 ± 0.003
GRC3	0.725 ± 0.001	0.430 ± 0.003

Abbreviations: n.d., not determined.

The VLB120 wildtype had a growth rate of 0.625 ± 0.003 h^{-1} and a biomass yield coefficient of 0.372 ± 0.003 g_{cdw} $g_{glucose}^{-1}$, which is close to the values reported by Volmer et al. [61] for the same wildtype strain in a different mineral medium (μ = 0.53 h^{-1} and $Y_{X/S}$ = 0.36 g_{CDW} $g_{glucose}^{-1}$). VLB120ΔpSTY served as a control since all other tested strains had lost the megaplasmid during the DNA deletion processes. The deletion of the pSTY megaplasmid had no significant effect on the biomass yield. Yet, the growth rate was significantly increased. The pSTY megaplasmid represents a large proportion of the total genome of *P. taiwanensis* VLB120 with a size of 321.7 kb and 365 identified coding sequences (CDS)[65]. The elevated growth rate likely results from a combinatory relief concerning DNA replication, transcription, and translation since DNA synthesis alone accounts for less than 0.1% of the total cellular ATP demand[20,66].

The following strains were compared to VLB120ΔpSTY regarding their growth rate, and to the wildtype regarding the biomass yield coefficient as the latter was unaffected from the deletion of pSTY. The individual deletion of the flagellar segments flag1 and flag2 as well as Δ*fliL* significantly elevated the biomass yield ($p < 0.02$). VLB120Δflagella pSTY$^-$, which comprises Δflag1 and Δflag2, showed an increased biomass yield that was comparable to the one of VLB120Δflag1 pSTY$^-$, but higher than the one of VLB120Δflag2 pSTY$^-$. The deletion of the flagellar apparatus in its entirety thus poses a large benefit for planktonic cells in biotechnological processes as there is no need to costly synthesize and operate flagella in well-mixed shake flasks or stirred bioreactors. In *E. coli*, roughly 2% of the cell's biosynthetic energy is required for the flagellar synthesis while another 0.1% of the total energy cost is consumed for the operation of the flagella[37,39]. Accordingly, VLB120Δflagella also featured a significantly increased ($p < 0.005$) growth rate. In *P. putida* KT2440, the elimination of the flagellar cluster increased the growth rate by 24% in shake flask cultures[22]. The determined growth rate of VLB120Δflagella pSTY$^-$ was increased by 16% compared to VLB120ΔpSTY. Of strains VLB120Δ*fliL* pSTY$^-$, VLB120Δflag1 pSTY$^-$, and VLB120Δflag2 pSTY$^-$, all but VLB120Δflag1 feature lower biomass yields than VLB120Δflagella pSTY$^-$, indicating that deletion of the flag1 cluster is the main contributor to the increase in biomass yield, but also suggesting that it is beneficial to remove the complete flagellar cluster rather than only parts or single genes (Table 2).

The elimination of biofilm-associated proteins by clearance of the three *lap* regions had an apparent negative effect on the growth rate. In spite of this, strain VLB120ΔflagellaΔlap1/2/3 pSTY$^-$ was the first to reach the stationary phase as seen in Figure 4B. A *P. putida* Δ*lapA*Δ*lapF* double mutant showed similar dynamics, which was attributed to a decreased lag phase[59]. These observations could be due to the formation of microcolony-like cell clusters caused by cell-cell attachment in the lap1/2/3-positive strains (J. Klebensberger, personal communication). The initial OD_{600} of 0.05 dropped within 1 h to ≤ 0.02 for all strains with intact *lap* clusters, while it only marginally decreased for VLB120Δlap1/2/3 pSTY$^-$ and even increased in case of VLB120ΔflagellaΔlap1/2/3 pSTY$^-$. This observation is more visible on a logarithmic scale (Figu S2, supplemental information). The resuspension of flocculent cell aggregates could result in an OD_{600} increase that is not related to an actual gain of biomass. Therefore, the relatively high growth rates determined for VLB120Δflagella pSTY$^-$ and other *lap*-positive strains could be a result of overestimation.

Strain VLB120Δlap1/2/3 pSTY$^-$ showed an increased biomass yield ($p < 0.002$), which could be due to a relief regarding protein expression. Especially the elimination of the *lap* region-encoded large adhesive proteins LapA and LapF likely causes a reduced burden as they are the first and second largest proteins in *P. putida* KT2440 with 8682 and 6310 amino acids (aa), respectively[67]. In *P. taiwanensis* VLB120, the respective homologues are also very large (LapA: 4032 aa; LapF: 3590 aa), yet much smaller compared to the respective proteins in *P. putida* KT2440. The combinatorial deletion of Δflag1/Δflag2 and Δlap1/Δlap2/Δlap3 did not lead to a further increase regarding the biomass yield coefficient.

2.5. TtgGHI transplantation and deletion of proviral DNA segments

With roughly 5.39%, the pSTY megaplasmid accounts for a large portion of the genomic DNA of *P. taiwanensis* VLB120[65]. It comprises many mobile elements that pose a potential cause of genetic instability. Additionally, only a very small number of encoded genes are relevant for industrial biotechnology. Surely, of greatest interest is the pSTY-encoded efflux pump TtgGHI, but also the styrene degrading pathway has been used for biotransformation of styrene to (*S*)-styrene oxide[25, 31].

In Section 2.4, it was shown that the elimination of pSTY resulted in an increased growth rate, thus making the pSTY elimination attractive for laboratory and industrial applications. However, the elimination of pSTY led to solvent sensitivity (Figure 3A), and solvent tolerance is a key feature we wanted to retain. Moreover, the pSTY megaplasmid got lost quite frequently during the process of strain engineering using established conjugational plasmid delivery techniques. This genetic instability is inconvenient during genetic engineering if one wants to maintain features conveyed by the megaplasmid. We therefore opted for chromosomal transplantation of *ttg(VW)GHI* to re-establish tolerance towards hydrophobic solvents.

Proviral sequences display additional superfluous or burdensome DNA components that can eventually become harmful under certain circumstances such as stress-triggering conditions[68], since complete prophages can re-enter the lytic cycle and kill the cell[21]. However, in some cases the prophage might also encode beneficial features[69]. Certainly, phages contribute to an increased genetic diversity, which can be beneficial in the sense of adaptive evolution[21]. However, in laboratory and industrial biotechnology settings a genetic stability is usually desired, since instability affects reproducibility and large-scale fermentations often involve many generations from seed to harvest. For this reason, we aimed to delete large proviral DNA segments. According to PHASTER[70], *P. taiwanensis* VLB120 harbors five large prophagic DNA segments. The exact position and genetic composition of the prophages is given in the supplemental information (Table S3 and S4). Table 1 indicates the target regions as they were deleted and Table S4 gives a detailed overview of all CDS within the proviral segments and whether they were eliminated or not. Prophage 1, 3, and 5 are predicted to be intact, while prophage 2 is questionable and prophage 4 is incomplete[70]. Since the prophagic region 1 and 2 overlap, they were eliminated as a single deletion.

To re-establish solvent tolerance towards aromatic solvents, the structural efflux pump genes *ttgGHI* and the regulatory genes *ttgVW* were chromosomally integrated at the Δpro1/2 locus in the VLB120ΔpSTY mutant background. As previously reported, the deletion of *ttgV* led to a constitutive solvent tolerance in *P. taiwanensis* VLB120[61]. Therefore, we also replaced pro1/2 by *ttgGHI* only, omitting *ttgVW*. The putative anti-repressor-encoding gene *ttgW*[61] that was shown to have no major role in the regulation of the TtgGHI efflux pump in *P. putida* DOT-T1E[71] is predicted to be superfluous in a strain lacking TtgV. The *ttg(VW)GHI* cassettes were integrated into the pEMG-pro1/2 deletion delivery vector in-between TS1 and TS2. Their use led to a substitution of the chromosomal pro1/2 sequence with *ttg(VW)GHI*. In the background of VLB120ΔpSTYΔpro1/2::*ttgGHI*, the remaining proviral segments pro3, pro4, and pro5 were consecutively deleted. The deletion of pro5 could only be achieved by integration of a *tetA* marker using the delivery plasmid pEMGu-pro5-*tetA*. The *tetA* marker was subsequently removed in a consecutive deletion process using the pEMGu-pro5 plasmid.

To assess the effect of the elimination of the prophagic elements on growth, the consecutive prophage deletion strains were grown in MSM with 20 mM glucose and their growth kinetics were recorded using the CGQ. The deletion of pro1/2, pro3, and pro4 did not cause a significant change regarding growth behavior (Figure S3, supplemental information) as the corresponding strains showed almost the same growth curve as the reference strain VLB120ΔpSTY, despite the fact that constitutive expression of the TtgGHI efflux pump could potentially be disadvantageous. Indeed, strain VLB120Δpro1/2::*ttgVWGHI* that harbors the regulators TtgV and TtgW for inducible solvent tolerance seemed to have a small growth advantage (Figure S3, supplemental information). A more detailed investigation on the effect of inducible versus constitutive solvent tolerance will be given below for the final genome-reduced chassis strains.

VLB120Δpro1/2::*ttgGHI*Δpro3Δpro4Δpro5 had a significantly impaired growth rate (Figure S3, supplemental information) and biomass yield (Table S5, supplemental information). The deleted proportion of prophage 5 only included proviral- or transposon-associated and hypothetical genes (Table S4, supplemental information). Further investigations to identify the reason for the growth defect are beyond the scope of this study, but the growth phenotype reveals that there must be a factor contributing to the fitness of *P. taiwanensis* VLB120 under the tested conditions, likely explaining the challenges encountered in obtaining the respective deletion. This is in contrast to *P. putida* KT2440Δall-Φ, in which no disadvantages could be assigned to the removal of the proviral segments despite a detailed characterization under various conditions[21]. Freeing this strain from its proviral load resulted in the generation of a more robust and physiologically better performing strain (KT2440Δall-Φ), featuring an increased resistance towards DNA damage and oxidative stress. A similar effect can be expected from the removal of prophages from *P. taiwanensis* VLB120, with the exception of prophage 5, the removal

of which provides a disadvantage to the cell. Hence, the pro5 segment was retained in further streamlined chassis strains.

2.6. Genome reduction

In the course of this study, the two streamlined strain lines VLB120ΔflagellaΔlap1/2/3 pSTY⁻ and VLB120ΔpSTY::*ttgGHI*Δpro1/2Δpro3Δ4 were generated. To combine the beneficial traits of these two strains, the Δflag1/Δflag2 and lap1/Δlap2/Δlap3 modifications were introduced into VLB120ΔpSTYΔpro1/2::*ttgGHI*Δpro3Δpro4 to yield GRC2. Its isogenic variants harboring the Δpro1/2 and Δpro1/2*::ttgVWGHI* modifications were derived from this strain to yield GRC1 and GRC3, respectively. Figure S4 in the supplemental information illustrates the genealogy of the generated chassis strains.

Once again, these strains were assessed for their growth kinetics on MSM supplemented with 20 mM glucose. Growth rates and biomass yield coefficients for GRC1, GRC2, and GRC3 are given in Table 2. Figure 5 shows the growth kinetics obtained by manually sampled growth curves (Figure 5A) and by the CGQ (Figure 5B).

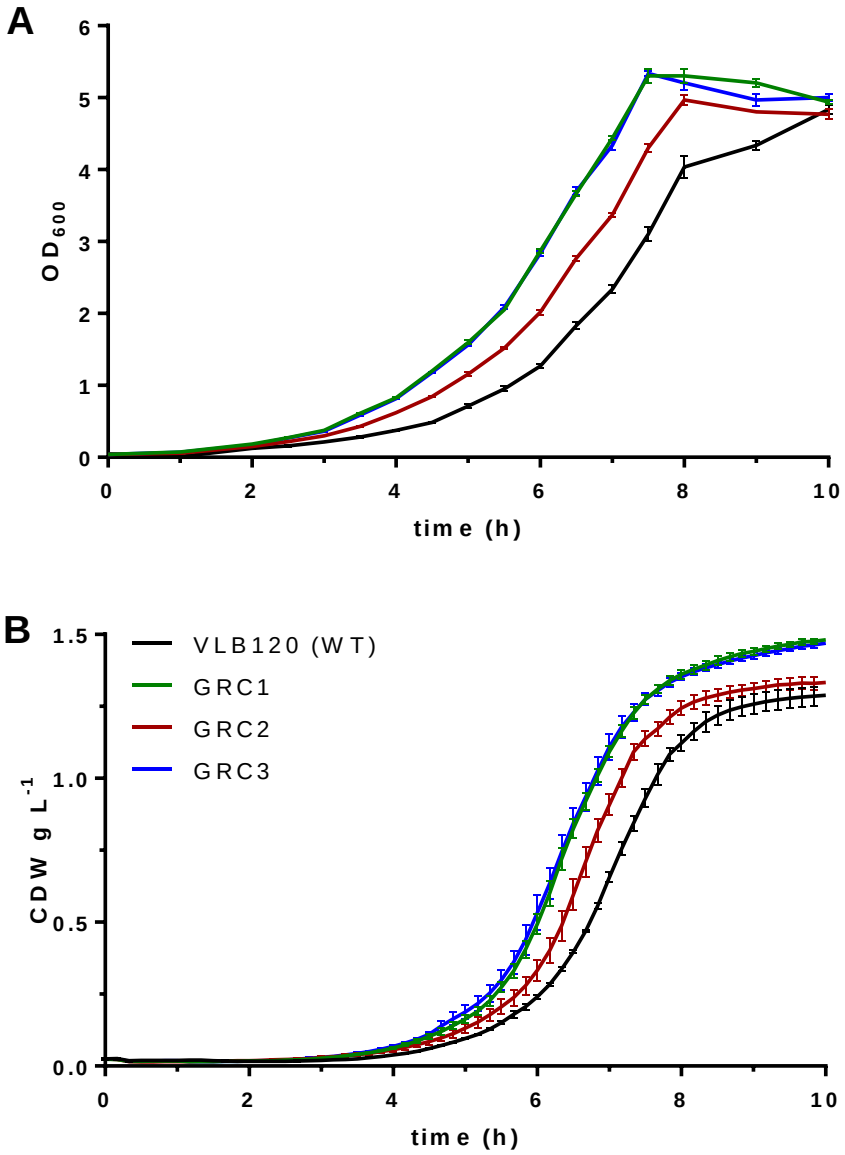

Figure 5. Growth of *P. taiwanensis* GRC1, GRC2, and GRC3 in shake flasks with MSM with 20 mM glucose obtained by manual sampling with offline measurement of the OD_{600} (A) and by the CGQ with online scattered light measurement converted into CDW using end point biomass yields obtained for the respective cultures (B). Error bars indicate the standard error of the mean (n = 3). The growth curve for the wildtype shown in (A) was taken from Figure 5A and serves as reference.

The growth rates and biomass yields of GRC1 and GRC3 did not show a significant difference (Table 2), indicating that the inducible solvent tolerance of GRC3 poses no burden due to transcriptional repression of *ttgGHI* conveyed by TtgV. The constitutively solvent-tolerant strain GRC2, however, grew

significantly slower ($p < 0.02$) and had a lower biomass yield ($p < 0.002$). Yet, this strain still showed better performances than the wildtype concerning both growth rate and biomass yield (Table 2). Compared to VLB120ΔflagellaΔlap1Δlap2Δlap3 pSTY^{-}, the growth rates of GRC1 and GRC3 were not further increased and the biomass yield coefficients were within the same range, except for GRC1, which showed a small but significant increase ($p < 0.05$). For the previously engineered constitutively solvent-tolerant *P. taiwanensis* VLB120Δ*C*Δ*ttgV* described by Volmer et al.[61] only a minor decrease regarding growth rate (from $\mu = 0.56$ to 0.53 h^{-1}) and biomass yield (from $Y_{X/S} = 0.36$ to 0.35 $g_{CDW}\ g_{glucose}^{-1}$) was reported. In this study, the difference between constitutive and inducible solvent tolerance was more prominent, which may be related to the fact that the GRC background provides a higher baseline growth rate than the wildtype.

To verify the solvent tolerance of the GRC1, GRC2, and GRC3, these strains and the reference strains VLB120 and VLB120ΔpSTY were exposed to toluene applying the previously described plate overlay assay. The growth of the respective strains under a layer of toluene can be seen in Figure 6.

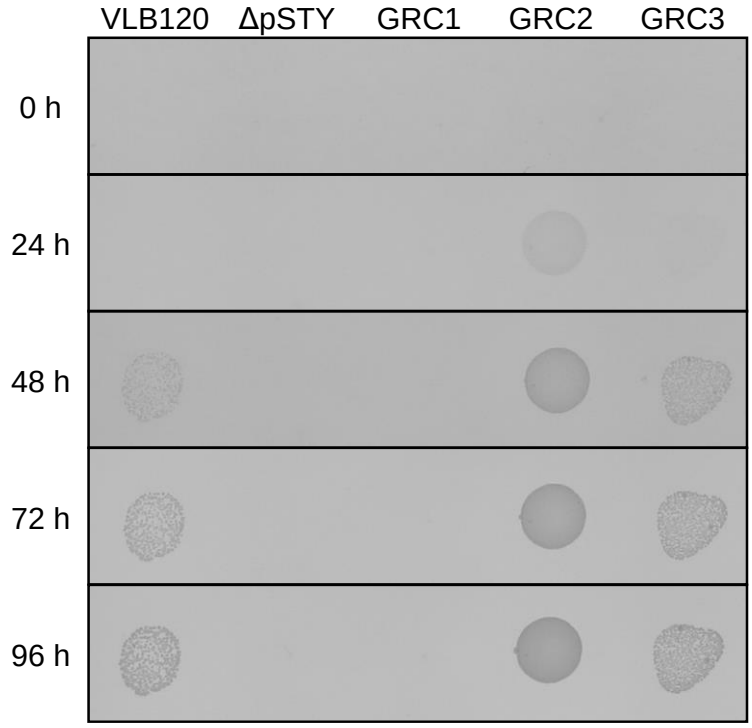

Figure 6. Growth of *P. taiwanensis* VLB120 wildtype and strain ΔpSTY, GRC1, GRC2, and GRC3 on LB agar plates exposed to styrene vapor for 6 h and subsequently covered with 70 mL of liquid toluene at room temperature. A cell suspension volume of 10 µL with an OD_{600} of ~0.01 was spotted. One representative dataset of three replicates is shown.

After an incubation of 24 h, only strain GRC2 showed visually detectable growth, indicating an increased solvent tolerance. After 48 h, also the wildtype and GRC3 showed growth, although less distinct than that of GRC2. At this point, GRC2 spots formed a lawn, while VLB120 (WT) and GRC3 spots only showed single colony formation. This indicates that despite an adaptation for 6 h in a saturated styrene vapor phase, neither VLB120 (WT) nor GRC3 are fully adapted to solvents, or that GRC2's tolerance was enhanced above the level of the strains harboring the machinery for *ttgGHI* transcriptional repression. Volmer et al.[61] showed that constitutive solvent tolerance renders cumbersome adaptation procedures unnecessary and reported increased styrene epoxidation activity in a constitutively solvent-tolerant strain. However, in GRC2 there is a trade-off between solvent tolerance and growth fitness (lowered biomass yield and growth rate) without the presence of organic solvents. Hence, GRC2 is only a suitable chassis in the context of solvent tolerance and not for broad applications. The difference between GRC3 and VLB120 (WT) was indistinguishable with this semi-quantitative assay.

To further investigate solvent tolerance the genome-reduced chassis strains and the control strains VLB120 (WT) and VLB120ΔpSTY were grown in a liquid system of MSM supplemented with 20 mM glucose in the presence of 5 mM 4-ethylphenol (4-EP) or phenol. For 4-EP, the main cultures were inoculated from MSM pre-cultures with 20 mM glucose and 1 mM 4-EP for adaptation. Cell densities were measured online as scattered light using the CGQ and converted to OD_{600} by means of a calibration

curve (Figure 7A). 4-EP has a log P_{ow} value of 2.50, which is similar to that of toluene (2.73)[72]. Therefore, it poses a similar toxicity and mode of action. In contrast, phenol is a chaotropic solute that features a higher water solubility and lower log P_{ow} (1.50)[72]. While VLB120ΔpSTY and strain GRC1 were able to grow in the pre-culture withstanding a concentration of 1 mM 4-EP, they were unable to grow in the main culture with this compound. Strains GRC2, GRC3, and the wildtype did grow in the presence of 5 mM 4-EP with a pattern that confirmed the plate-overlay assay. Despite the presence of 1 mM 4-EP in the pre-culture and the resulting solvent adaptation, GRC3 and the wildtype showed long lag phases of approximately 19.5 and 24.5 h, respectively, while GRC2 had a much shorter lag phase (~4.5 h). The fact that GRC3 had a shorter lag phase than the wildtype indicates that the general advantages of the genome-reduced chassis strain are also beneficial under solvent stress.

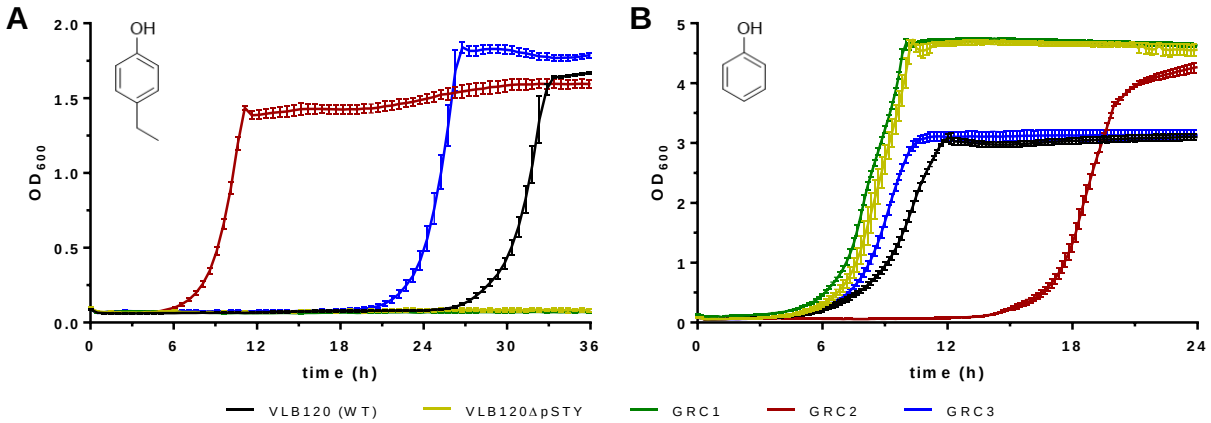

Figure 7. Growth of *P. taiwanensis* VLB120 (WT), VLB120ΔpSTY, GRC1, GRC2, and GRC3 in MSM with 20 mM glucose and 5 mM 4-ethylphenol (4-EP) after adaptation (A) or 5 mM phenol without prior adaptation (B). Growth kinetics were obtained using the CGQ with online scattered light measurement converted into OD_{600} using a calibration**.** Error bars indicate the standard error of the mean (n = 3).

In stark contrast, the expression of TtgGHI reduced the tolerance towards phenol. GRC2, which constitutively expresses this extrusion pump, showed a prolonged lag phase of approximately 13 h, while GRC1 – the same strain lacking TtgGHI – showed good growth and reached the stationary phase already after 10 h. GRC3, which inducibly expresses TtgGHI, showed an intermediate phenotype, although its final OD_{600} (3.13 ± 0.09) was lower than that of GRC2 (4.27 ± 0.09). For *P. putida* KT2440 the deletion of *ttgABC*, which encodes a related efflux pump that is upregulated in the presence of phenol[73], was previously shown to increase phenol tolerance[74]. The negative impact of TtgGHI on phenol tolerance of *P. taiwanensis* was confirmed by the growth behavior of the wildtype and the ΔpSTY control strain. While ΔpSTY showed nearly the same kinetics as GRC1, the wildtype's growth was delayed and the final optical density (3.10 ± 0.06) was decreased.

One hypothesis for the negative impact of TtgGHI expression on phenol tolerance is that phenol diffuses back into the cell at a higher rate, leading to a futile cycle of secretion and uptake. One indication for this is the effect of OprB-1 deletion. This glucose porin is speculated to facilitate phenol uptake[75,76]. The deletion of *oprB-1* did not affect phenol production in previously engineered producers[35], but the disruption of *oprB-1* was shown to increase phenol tolerance in *P. putida* KT2440[76]. Consistently, the deletion of *oprB-1* enhanced the tolerance towards phenol in the background of GRC2 and GRC3, but not in GRC1 lacking TtgGHI (Figure S5, supplemental information). However, also with *oprB-1* deletion, GRC1 is still the most tolerant towards phenol. Possibly, OprB-1 permits passage of this more hydrophobic molecule, thereby facilitating reuptake through the outer membrane and negating adaptive responses at this barrier.

Altogether, the stark performance differences of GRC1, GRC2, and GRC3 on these two relatively similar molecules highlights the need for having multiple variants that differ in their solvent tolerance, enabling the *à la carte* selection of the most appropriate chassis.

2.7. Metabolic engineering for the comparative production of phenol

In order to assess the added value of the GRC strains' improved process features in a biotechnological application the most crucial genetic modifications identified by Wynands et al.[35] for the production of tyrosine-derived aromatics were introduced into GRC1. These included the deletion

of *pobA*, *hpd*, *quiC*, *quiC1*, and *quiC2* (= Δ5) to prevent precursor degradation and the modifications *trpE*^{P290S}, *aroF-1*^{P148L}, *pheA*^{T310I}, Δ*pykA*, and *attTn7::P*$_{14g}$*-PaTPL2-aroG*^{fbr}*-tyrA*^{fbr} to increase the flux towards tyrosine and enable phenol production, introduced using the same methodologies and plasmids applied in Wynands et al.[35]. However, for a more time-efficient engineering, the genes *pobA*, *hpd*, and *quiC1* were deleted in a single deletion procedure. Additionally, *ppc* (PVLB_19630) was deleted since this was found to further improve phenol production in a separate study. The resulting strain was denoted GRC1Δ5-TPL38. Subsequently, this strain and the non-streamlined equivalent VLB120Δ5-TPL38 (derived from VLB120Δ5-TPL36 by deletion of *ppc*) were cultured in MSM with 40 mM glycerol. The corresponding growth, phenol production, and glycerol consumption is shown in Figure 8.

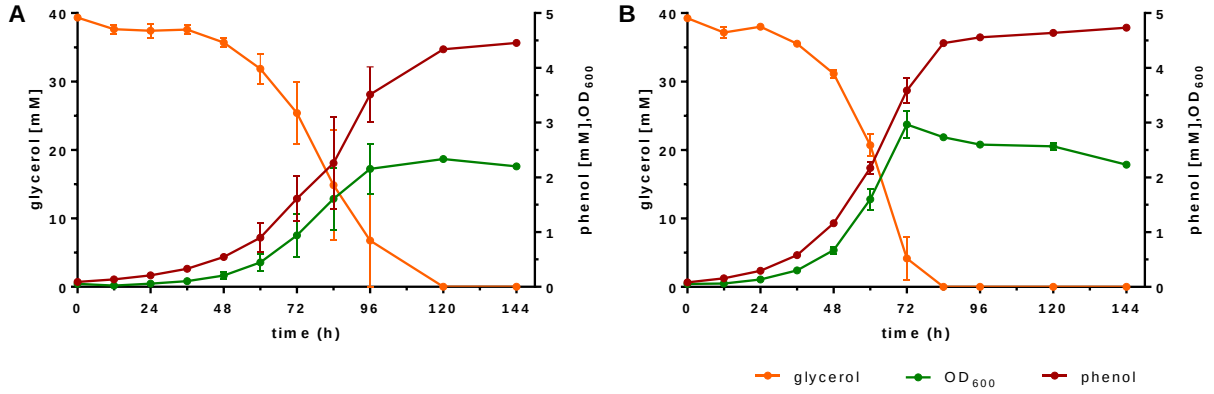

Figure 8. Phenol production of *P. taiwanensis* VLB120Δ5-TPL38 and GRC1Δ5-TPL38 from glycerol. The OD_{600}, phenol production, and glycerol consumption is plotted over time for VLB120Δ5-TPL38 (A) and GRC1-TPL38 (B). The cultures were grown in Boston shake flasks with MSM supplemented with 40 mM glycerol. Error bars indicate the standard error of the mean (n = 3).

Under these conditions, the growth rate of GRC1Δ5-TPL38 was 0.07 ± 0.00 h^{-1} and that of VLB120Δ5-TPL38 was 0.06 ± 0.01 h^{-1}. The GRC1-based producer reached a higher maximum OD_{600} of 3.0 ± 0.24 compared to 2.3 ± 0.03 for VLB120Δ5-TPL38, and the substrate was completely consumed in 84 h by the GRC1 strain, and in 120 h by the VLB120 equivalent. This increased substrate uptake rate also resulted in a 1.47-fold increased volumetric production rate of 0.052 ± 0.000 mM h^{-1} with GRC1Δ5-TPL38 (between 0 and 84 h of cultivation), compared to VLB120Δ5-TPL38 which only reached 0.035 ± 0.000 mM h^{-1} (between 0 and 120 h of cultivation). The maximum phenol titer of 4.74 ± 0.02 mM achieved by GRC1Δ5-TPL38 is also significantly higher than that of VLB120Δ5-TPL38 (4.46 ± 0.04 mM), which translates into an equivalently higher yield of 24.1 ± 0.2% compared to 22.7 ± 0.2% (Cmol/Cmol).

Overall, the GRC1 strain outperformed the non-streamlined chassis on all key performance indicators, with the greatest benefit observed for the production rate. In part, this can also be attributed to a distinctly sigmoidial trend in phenol production of strain VLB120Δ5-TPL38, likely due to phenol stress towards the end of the culture. In contrast, the more phenol-resistent GRC1 did not show this trend.

3. Conclusions

In this study, we generated streamlined chassis strains of solvent-tolerant *P. taiwanensis* VLB120 by targeted elimination of large DNA segments encoding dispensable or unfavorable cell functions including the megaplasmid pSTY, large proviral segments, and large flagellar- and biofilm-associated gene clusters. The final GRC strains feature a genome reduced by approximately 10% and enhanced performances relevant to many industrial applications. We eliminated the strains' ability to swim and to form biofilm, as these cell functions are unfavorable under most biotechnological settings. However, under specific process settings, e.g., catalytic biofilms, some of these features could be desired. The process-guided utilization of custom-tailored platform strains chosen from a set of different chassis, endowed with various trait combinations such as tolerance, behavior, efficiency, and stability, allows the selection of a microbial host *à la carte* according to the bioprocess requirements. The here generated GRC strains exemplify this principle. While some of their enhanced key performance indicators including increased growth rates and biomass yields are likely beneficial for a broad range of applications, the desired solvent tolerance level should be chosen according to the intended product and process. This study provides a basis for forthcoming chassis engineering efforts to expand the repertoire

of strains. It also enables the more efficient production of a range of both toxic and non-toxic value-added chemicals, as exemplified for phenol, thereby moving *P. taiwanensis* VLB120 even closer towards industrial application.

4. Experimental procedures

4.1. Media and culture conditions

E. coli and *P. taiwanensis* VLB120 strains were routinely grown in lysogeny broth (LB) medium containing 10 g L^{-1} peptone, 5 g L^{-1} sodium chloride, and 5 g L^{-1} yeast extract at 37 and 30°C, respectively. Cetrimide agar (Sigma-Aldrich, St. Louis, MO, USA) was used as selective medium for the isolation of *P. taiwanensis* after mating procedures. Growth and characterization experiments were performed using mineral salt medium (MSM) according to Hartmans et al.[77] unless stated otherwise. Main cultures were inoculated from liquid pre-cultures to an approximate OD_{600} of 0.05 unless stated otherwise. Solid medium plates of LB and MSM were prepared by addition of 1.5% agar. Antibiotics were supplemented to the medium as required to grant selection or maintenance of delivered genetic elements. For *P. taiwanensis*, tetracycline hydrochloride and spectinomycin hydrochloride pentahydrate were applied at concentrations of 60 and 800 mg L^{-1}, respectively, while for *E. coli* only 10 and 50 mg L^{-1} of the corresponding antibiotic were used. The kanamycin sulfate concentration was 50 mg L^{-1} independent from the bacterial species cultured. The gentamicin concentration was set to 10 mg L^{-1} for solid and liquid cultures of *E. coli* and liquid cultures of *P. taiwanensis*, whereas 25 mg L^{-1} were used when *P. taiwanensis* was grown on solid medium. *E. coli* DH5α λpir pTNS1 was grown with 100 mg L^{-1} ampicillin. For the conjugational reintegration of the pSTY megaplasmid or the verification of its presence 5 mg L^{-1} mercury(II) chloride (Sigma-Aldrich) was added to the medium to yield selective conditions as pSTY mediates mercury resistance[65]. Liquid cultures were grown in a horizontal orbital shaker with a throw of 50 mm and a frequency of 200 rpm when shake flasks were used for cultivation. The pre-cultures for the plate-based solvent tolerance assays were cultivated using the System-Duetz (Enzyscreen, Heemstede, the Netherlands) in 24-square deep well plates[78] with a filling volume of 1.5 mL shaking with 300 rpm. The chemicals used in this study were obtained from either Carl Roth (Karlsruhe, Germany), Sigma-Aldrich (St. Louis, MO, USA), or Merck (Darmstadt, Germany) if not explicitly declared differently. D-(+)-glucose monohydrate (Carl Roth) was used as carbon and energy source in multiple experiments. For the evaluation of solvent tolerance toluene (Sigma-Aldrich) or 4-ethylphenol (Sigma-Aldrich) was used. Styrene (Sigma-Aldrich, ≥99%, stabilized with 4-*tert*-butylcatechol) was used as carbon source and inducer for the TtgGHI efflux pump expression, in which cases it was provided via the vapor phase.

For the investigation of growth kinetics, selected strains were grown in MSM supplemented with 20 mM glucose using 500 mL shake flasks filled with 25 mL medium. Cell growth was analyzed either by sampling and offline OD_{600} measurement, or by non-invasive online backscatter measurement using the cell growth quantifier (CGQ, aquila biolabs GmbH, Baesweiler, Germany).

Phenol production experiments were performed in mineral salt medium with 40 mM glycerol as sole carbon source using Boston bottles with Mininert valves (Thermo Fisher Scientific, Waltham, Mam USA) under the same conditions described by Wynands et al.[35].

4.2. Plasmid cloning and strain engineering

All plasmids assembled within this study were constructed by either standard restriction-ligation procedures or Gibson cloning[79] using the NEBuilder HiFi DNA Assembly (New England Biolabs, Ipswich, MA, USA). DNA modifying enzymes and polymerases were purchased from either Thermo Fisher Scientific or New England Biolabs. PCR primers were ordered as unmodified DNA oligonucleotides from Eurofins Genomics (Ebersberg, Germany). A list containing all primers used for cloning can be found within the supplemental information (Table S6). The PCR amplification of DNA as part of cloning procedures was realized using the Q5 High-Fidelity Polymerase. Plasmid delivery was achieved by electroporation using a GenePulser Xcell (BioRad, Hercules, CA, USA) (settings: 2 mm cuvette gap, 2.5 kV, 200 Ω, 25 μF) or alternatively in case of mobilizable vectors into *Pseudomonas* by conjugation. Conjugations were accomplished in mating procedures as described in Wynands et al.[35]. The correct assembly of cloned plasmids, obtained deletions, genomic replacements, successful mini-Tn7 transposon deliveries, and pSTY re-integration were verified by colony PCR using the One*Taq* 2X Master Mix with Standard Buffer. To enhance the efficiency, template cell material was lysed in alkaline polyethylene glycol according to Chomczynski and Rymaszewski[80] prior to its use as template

in colony PCR. The inserts of cloned plasmids and PCR products obtained from the mapping of gene deletions were confirmed by Sanger sequencing executed by Eurofins Genomics.

For the generation of seamless DNA deletions and point mutations the I-SceI-based system developed by Martínez-García and Lorenzo[81] was used according to the streamlined protocol described in Wynands et al.[35]. The 400-1000 bp up- and downstream flanking regions, denoted as TS1 and TS2, of the deletion target were integrated into the suicide delivery vector pEMG, pEMGu, pEMGg, pSEVA412S, or pSEVA512S (kindly donated by V. de Lorenzo) whose multiple cloning sites are each flanked by two I-SceI restriction sites. Positive clones were iteratively streaked onto unselective LB agar plates several times to cure the strain from pSW-2 and segregate contaminative impurities. The correct genotype was re-confirmed by diagnostic colony PCR. For the chromosomal integration of the natively pSTY-located efflux pump encoding genes, *ttgVWGHI*- and *ttgGHI*-encoding DNA sequences including the corresponding native promoters were integrated between TS1 and TS2 into the pEMG-pro1/2 deletion vector thereby obtaining pEMG-pro1/2-*ttgVWGHI* and pEMG-pro1/2-*ttgGHI*, respectively. The pSTY deletion was obtained using plasmid pEMG-pSTY, which only contains one TS sequence for homologous cointegration into the megaplasmid. After I-SceI-mediated introduction of DNA double-strand breaks into pSTY, the loss of the megaplasmid was based on a failure of cell inherent repair mechanisms.

In the metabolic engineering approach the modifications Δ*pobA*, Δ*hpd*, Δ*quiC*, Δ*quiC1*, Δ*quiC2*, *trpE*^{P290S}, *aroF-1*^{P148L}, *pheA*^{T310I}, Δ*pykA*, and *attTn7::P*$_{14g}$*-PaTPL2-aroG*^{fbr}*-tyrA*^{fbr} were introduced using the same methodologies and plasmids applied in Wynands et al.[35] with the exception that *quiC1*, *hpd*, and *pobA* were eliminated in a single deletion procedure. For this purpose, the plasmids pSEVA412S-*quiC1*, pSEVA512S-*hpd*, and pEMG-*pobA* were successively integrated into the genome. The resolution of all three cointegrates was achieved by a single delivery of the I-SceI-expression plasmid pSW-2.

For the genomic integration of a gentamicin-resistance marker the pBG42 mini-Tn7 transposon delivery plasmid containing a bicistronic cassette for constitutive expression of *msfgfp* was used [63]. The cassette's targeted integration into the Tn7 attachment site was accomplished by mating procedures including the *E. coli* PIR2 pBG42 donor, the *E. coli* HB101 pRK2013 helper, the *Pseudomonas* recipient, and the transposase providing strain *E. coli* DH5α λpir pTNS1. For the conjugational re-integration of pSTY into strains that had lost this megaplasmid the gentamicin resistance conveyed by the genomic integration of the pBG42-encoded mini-Tn7 transposon was used as selection marker in the background of the *P. taiwanensis* VLB120 wildtype used as pSTY donor. pSTY is a conjugative plasmid, thus the use of a helper strain was not needed. Its transfer was selected by means of mercury resistance.

A full list of all strains used and obtained within this work can be found in Table 3.

Table 3 Bacterial strains used in this study.

Strain	Relevant characteristics	Reference
E. coli		
DH5α	*supE44*, Δ*lacU169* (*φ80lacZ*ΔM15), *hsdR17* ($r_K^-m_K^+$), *recA1*, *endA1*, *gyrA96*, *thi-1*, *relA1*	Hanahan[82]
DH5α λpir	λ*pir* lysogen of DH5α; host for *oriV*(R6K) vectors	de Lorenzo and Timmis[83]
HB101 pRK2013	Sm^R, *hsdR-M*$^+$, *proA2*, *leuB6*, *thi-1*, *recA*; bears plasmid pRK2013	Ditta et al.[84]
DH5α pSW-2	DH5α bearing pSW-2	Martínez-García and de Lorenzo[40]
PIR2 pBG42	F$^-$, Δ*lac169*, *rpoS(Am)*, *robA1*, *creC510*, *hsdR514*, *endA*, *recA1uidA(*Δ*MluI)*::*pir*; bears plasmid pBG42	Zobel et al.[63]
DH5α λpir pTNS1	DH5α λpir bearing plasmid pTNS1	de Lorenzo lab
P. taiwanensis		
VLB120	wildtype	Panke et al.[25]
VLB120ΔpSTY	ΔpSTY	this study
VLB120Δ*fliL*	Δ*fliL*, pSTY$^-$	this study
VLB120Δflag1	Δflag1 (PVLB_17040-17260), pSTY$^-$	this study
VLB120Δflag2	Δflag2 (PVLB_17340-17425), pSTY$^-$	this study
VLB120Δflagella	Δflag1Δflag2, pSTY$^-$	this study
VLB120Δflagella pSTY$^+$	Δflag1, Δflag2, pSTY$^+$	this study
VLB120Δflagella-BG42 pSTY$^+$	Δflag1, Δflag2, *attTn7*::P_{14g}-*msfgfp*, pSTY$^+$	this study
VLB120Δlap1/2	Δlap1 (PVLB_00915-40), Δlap2 (PVLB_17755-85), pSTY$^-$	this study
VLB120Δlap1/2/3	Δlap1, Δlap2, Δlap3 (4601770 bp to PVLB_20985), pSTY$^-$	this study
VLB120Δlap1/2/3-BG42 pSTY$^+$	Δlap1, Δlap2, Δlap3, *attTn7*::P_{14g}-*msfgfp*, pSTY$^+$	this study
VLB120ΔflagellaΔlap1/2/3	Δflag1, Δflag2, Δlap1, Δlap2, Δlap3, pSTY$^-$	this study
VLB120ΔflagellaΔlap1/2/3-BG42 pSTY$^+$	Δflag1, Δflag2, Δlap1, Δlap2, Δlap3, *attTn7*::P_{14g}-*msfgfp*, pSTY$^+$	this study
VLB120ΔpSTYΔpro1/2::*ttgVWGHI*	ΔpSTY, Δprophage1/2::*ttgVWGHI*	this study
VLB120ΔpSTYΔpro1/2::*ttgGHI*	ΔpSTY, Δprophage1/2::*ttgGHI*	this study
VLB120ΔpSTYΔpro1/2::*ttgGHI* Δpro3	ΔpSTY, Δprophage1/2::*ttgGHI*, Δprophage3	this study
VLB120ΔpSTYΔpro1/2::*ttgGHI* Δpro3Δpro4	ΔpSTY, Δprophage1/2::*ttgGHI*, Δprophage3, Δprophage4	this study

VLB120ΔpSTYΔpro1/2::*ttgGHI* Δpro3Δpro4Δpro5	ΔpSTY, Δprophage1/2::*ttgGHI*, Δprophage3, Δprophage4, Δprophage5	this study
GRC1	ΔpSTY, Δprophage1/2, Δprophage3, Δprophage4, Δflag1, Δflag2, Δlap1, Δlap2, Δlap3	this study
GRC2	ΔpSTY, Δprophage1/2::*ttgGHI*, Δprophage3, Δprophage4, Δflag1, Δflag2, Δlap1, Δlap2, Δlap3	this study
GRC3	ΔpSTY, Δprophage1/2::*VWGHI*, Δprophage3, Δprophage4, Δflag1, Δflag2, Δlap1, Δlap2, Δlap3	this study
GRC1Δ*oprB-1*	ΔpSTY, Δprophage1/2, Δprophage3, Δprophage4, Δflag1, Δflag2, Δlap1, Δlap2, Δlap3, Δ*oprB-1*	this study
GRC2Δ*oprB-1*	ΔpSTY, Δprophage1/2::*ttgGHI*, Δprophage3, Δprophage4, Δflag1, Δflag2, Δlap1, Δlap2, Δlap3, Δ*oprB-1*	this study
GRC3Δ*oprB-1*	ΔpSTY, Δprophage1/2::*VWGHI*, Δprophage3, Δprophage4, Δflag1, Δflag2, Δlap1, Δlap2, Δlap3, Δ*oprB-1*	this study
VLB120Δ5-TPL38	Δ*pobA*, Δ*hpd*, Δ*quiC*, Δ*quiC1*, Δ*quiC2*, $trpE^{P290S}$, $aroF\text{-}1^{P148L}$, $pheA^{T310I}$, Δ*pykA*, Δ*ppc*, $pSTY^{-}$, *attTn7*::P_{14g}-*PaTPL2*-$aroG^{fbr}$-$tyrA^{fbr}$	this study
GRC1Δ5-TPL38	GRC1 with Δ*pobA*, Δ*hpd*, Δ*quiC*, Δ*quiC1*, Δ*quiC2*, $trpE^{P290S}$, $aroF\text{-}1^{P148L}$, $pheA^{T310I}$, Δ*pykA*, Δ*ppc*, *attTn7*::P_{14g}-*PaTPL2*-$aroG^{fbr}$-$tyrA^{fbr}$	this study

4.3. Swim assay

Swimming behavior was assessed on MSM plates containing 20 mM glucose and 0.3% (w/v) agar. Pre-cultures grown in MSM with 20 mM glucose were diluted with a 0.9% (w/v) sodium chloride solution to yield suspensions with an OD_{600} of 0.05 whereof 2 µL was spotted into the middle of the soft agar plate. Swimming was scored after an incubation for 24, 48, and 72 h.

4.4. Biofilm formation assay

The assay used for the quantification of biofilm formation was based on a protocol from O'Toole[50]. LB pre-cultures of the investigated strains were used to inoculate MSM containing 20 mM glucose. The initial OD_{600} was set to 0.1 and 100 µL of the cultures were transferred to a polyvinyl chloride 96 well "U" bottom plate (Corning, Kennebunk, ME, USA). Thereafter, the plate surface was covered using a gas-permeable breathseal sealer (Greiner Bio-One, Frickenhausen, Germany) and the plate was stationarily incubated at 30°C for 10 h. The medium was discarded and the wells were washed with water, stained with crystal violet (Fluka, Buchs, Switzerland), washed again to remove exceeding dye, air-dried at room temperature, and photographed. To quantify the biofilm the dye was re-solubilized in 30% (v/v) acetic acid and the solution's absorbance was photometrically measured in a Synergy Mx microplate reader (BioTek Instruments, Winooski, VT, USA) at a wavelength of 550 nm. The experiment was performed in eight biological replicates.

4.5. Solvent tolerance tests

To study the tolerance of various strains towards toluene, LB pre-cultures were used to obtain cell suspensions of an OD_{600} of 0.01 by dilution with a 0.9% (w/v) sodium chloride solution. A volume of 10 µL was spotted onto LB agar in a glass Petri dish (⌀ 20 cm) and incubated at room temperature in a styrene saturated vapor phase in a large sealed desiccator to adapt the cells to solvent exposure. Then 70 mL of toluene was poured onto the plate, completely covering its surface.

To examine the solvent tolerance of selected strains in a liquid system, the respective strains were grown in MSM containing 20 mM glucose and 5 mM 4-ethylphenol. The main cultures were inoculated from MSM pre-cultures with 20 mM glucose and 1 mM 4-EP for the purpose of adaptation. Growth was profiled online as scattered light using the CGQ system (cell growth quantifier, aquila biolabs GmbH, Baesweiler, Germany). The same experiment was performed in the presence of 5 mM phenol instead of 4-EP. However, in this case main cultures were inoculated with unadapted pre-cultures.

4.6. Analytical methods

Optical densities of cell suspensions were measured at a wavelength of 600 nm using the Ultrospec 10 spectrophotometer (GE Healthcare, Chicago, IL, USA).

Online growth curves were obtained using the CGQ and CGQuant software (aquila biolabs GmbH). The CGQ measures the backscatter that can be converted into OD_{600} using a calibration obtained according to the manufacturer's instruction guide under consideration of the individual initial and final optical densities that were measured manually. If the biomass yield was determined in the end of the experiment, the OD_{600} was converted into cell dry weight (CDW).

For quantification of cell dry weights 24 mL of culture was pelleted, resuspended in Milli-Q water, and dried in a 1.5 mL glass vial at 60°C until the water was fully evaporated. The net cell dry weights were used for biomass yield calculations.

For the detection and quantification of phenol, sample supernatants were stored at −20°C until HPLC analysis in a 1260 Infinity II system (Agilent Technologies, Santa Clara, CA, USA) equipped with a 1260 DAD WR (Agilent Technologies) using a wavelength of 268 nm. A reversed phase HPLC column (ISAspher 100-5 C18 BDS, ISERA, Düren, Germany) was utilized and eluted with 0.1% (v/v) trifluoroacetic acid (TFA) and acetonitrile (Merck) at a flow rate of 0.8 mL min^{-1} for 20 min at a temperature of 40°C. The two eluents were applied in a constant starting ratio of 10% acetonitrile and 90% H_2O with 0.1% (v/v) TFA for the first 2 min. Thereafter, the proportion of acetonitrile was elevated to 95% within the next 10 min in a linear gradient and kept constant for the next 4 min, before it was gradually reduced to 10% within 2 min in a linear manner and kept constant for the rest of the run.

Glycerol concentrations were assessed by HPLC using a 1260 Infinity II (Agilent Technologies) equipped with a 1260 RID (Agilent Technologies). The column (Metab AAC, ISERA) was eluted with 5 mM H_2SO_4 at a constant flow of 0.5 mL min^{-1} and a temperature of 30°C for 20 min.

Errors are represented as standard error of the mean. Statistical significance was evaluated by *t*-test (two-tailed distribution, heteroscedastic, $p \leq 0.05$, if not stated differently).

Author contributions

N. W. conceived the project. B.W. and N.W. designed the experiments. B.W., N.R. and S.P. constructed all strains. N.R. performed the swimming assay. B.W. and N.R. performed the biofilm and toluene overlay assay. B.W. and S.P. charachterized the generated strains regarding their growth performance in liquid minimal medium with and without phenol and 4-ethylphenol. B.W. performed the phenol production experiment supported by M.O. All authors analyzed results. B.W. and N.W. wrote the manuscript with the help of M.O. and L.M.B.

Acknowledgements

This project was funded by the German Research Foundation through the Emmy Noether program (WI 4255/1-1). We gratefully acknowledge Prof. Dr. Víctor de Lorenzo (CSIC-CNB, Madrid) for providing us with strains and plasmids needed for the generation of deletion mutants. We thank Dr. Janosch Klebensberger (Institute of Biochemistry and Technical Biochemistry, University of Stuttgart) for the helpful discussion on microcolony formation and Christian Brüsseler (Institute of Bio- and Geosciences, IBG-1: Biotechnology, Forschungszentrum Jülich GmbH) for the assistance with the HPLC analysis.

References

[1] Becker, J., and Wittmann, C. (2015) Advanced biotechnology: metabolically engineered cells for the bio-based production of chemicals and fuels, materials, and health-care products, *Angew. Chem. Int. Ed. Engl. 54*, 3328-3350.

[2] Bailey, J. E. (1991) Toward a science of metabolic engineering, *Science. 252*, 1668-1675.

[3] Vickers, C. E., Blank, L. M., and Krömer, J. O. (2010) Grand challenge commentary: chassis cells for industrial biochemical production, *Nat. Chem. Biol. 6*, 875-877.

[4] Volmer, J., Schmid, A., and Bühler, B. (2015) Guiding bioprocess design by microbial ecology, *Curr. Opin. Microbiol. 25*, 25-32.

[5] Kolisnychenko, V., Plunkett, G., 3rd, Herring, C. D., Feher, T., Pósfai, J., Blattner, F. R., and Pósfai, G. (2002) Engineering a reduced *Escherichia coli* genome., *Genome Res. 12*, 640-647.

[6] Mizoguchi, H., Sawano, Y., Kato, J., and Mori, H. (2008) Superpositioning of deletions promotes growth of *Escherichia coli* with a reduced genome., *DNA Res. 15*, 277-284.

[7] Willrodt, C., Halan, B., Karthaus, L., Rehdorf, J., Julsing, M. K., Buehler, K., and Schmid, A. (2017) Continuous multistep synthesis of perillic acid from limonene by catalytic biofilms under segmented flow, *Biotechnol. Bioeng. 114*, 281-290.

[8] de Lorenzo, V. (2015) Chassis organism from *Corynebacterium glutamicum*: the way towards biotechnological domestication of Corynebacteria., *Biotechnol. J. 10*, 244-245.

[9] Nikel, P. I., Martinez-Garcia, E., and de Lorenzo, V. (2014) Biotechnological domestication of Pseudomonads using synthetic biology, *Nat. Rev. Micro. 12*, 368-379.

[10] Nikel, P. I., and de Lorenzo, V. (2018) *Pseudomonas putida* as a functional chassis for industrial biocatalysis: From native biochemistry to *trans*-metabolism, *Metab. Eng.*, Epub ahead of print.

[11] Martínez-García, E., and de Lorenzo, V. (2017) Molecular tools and emerging strategies for deep genetic/genomic refactoring of *Pseudomonas*, *Curr. Opin. Biotechnol. 47*, 120-132.

[12] Hirokawa, Y., Kawano, H., Tanaka-Masuda, K., Nakamura, N., Nakagawa, A., Ito, M., Mori, H., Oshima, T., and Ogasawara, N. (2013) Genetic manipulations restored the growth fitness of reduced-genome *Escherichia coli*, *J. Biosci. Bioeng 116*, 52-58.

[13] Umenhoffer, K., Feher, T., Baliko, G., Ayaydin, F., Pósfai, J., Blattner, F. R., and Pósfai, G. (2010) Reduced evolvability of *Escherichia coli* MDS42, an IS-less cellular chassis for molecular and synthetic biology applications., *Microb. Cell Fact. 9*, 38.

[14] Wenzel, M., and Altenbuchner, J. (2015) Development of a markerless gene deletion system for *Bacillus subtilis* based on the mannose phosphoenolpyruvate-dependent phosphotransferase system, *Microbiology 161*, 1942-1949.

[15] Westers, H., Dorenbos, R., van Dijl, J. M., Kabel, J., Flanagan, T., Devine, K. M., Jude, F., Séror, S. J., Beekman, A. C., Darmon, E., Eschevins, C., de Jong, A., Bron, S., Kuipers, O. P., Albertini, A. M., Antelmann, H., Hecker, M., Zamboni, N., Sauer, U., Bruand, C., Ehrlich, D. S., Alonso, J. C., Salas, M., and Quax, W. J. (2003) Genome engineering reveals large dispensable regions in *Bacillus subtilis*, *Mol. Biol. Evol 20*, 2076-2090.

[16] Baumgart, M., Unthan, S., Kloß, R., Radek, A., Polen, T., Tenhaef, N., Müller, M. F., Küberl, A., Siebert, D., Brühl, N., Marin, K., Hans, S., Krämer, R., Bott, M., Kalinowski, J., Wiechert, W., Seibold, G., Frunzke, J., Rückert, C., Wendisch, V. F., and Noack, S. (2018) *Corynebacterium glutamicum* chassis C1*: building and testing a novel platform host for synthetic biology and industrial biotechnology, *ACS Synth. Biol. 7*, 132-144.

[17] Martinez-Garcia, E., Nikel, P. I., Aparicio, T., and de Lorenzo, V. (2014) *Pseudomonas* 2.0: genetic upgrading of *P. putida* KT2440 as an enhanced host for heterologous gene expression, *Microb. Cell Fact. 13*, 159.

[18] Shen, X., Wang, Z., Huang, X., Hu, H., Wang, W., and Zhang, X. (2017) Developing genome-reduced *Pseudomonas chlororaphis* strains for the production of secondary metabolites, *BMC genomics 18*, 715.

[19] Csörgő, B., Fehér, T., Tímár, E., Blattner, F. R., and Pósfai, G. (2012) Low-mutation-rate, reduced-genome *Escherichia coli*: an improved host for faithful maintenance of engineered genetic constructs., *Microb. Cell Fact 11*, 11.

[20] Baumgart, M., Unthan, S., Rückert, C., Sivalingam, J., Grünberger, A., Kalinowski, J., Bott, M., Noack, S., and Frunzke, J. (2013) Construction of a prophage-free variant of *Corynebacterium glutamicum* ATCC 13032 for use as a platform strain for basic research and industrial biotechnology, *Appl. Environ. Microbiol. 79*, 6006-6015.

[21] Martinez-Garcia, E., Jatsenko, T., Kivisaar, M., and de Lorenzo, V. (2015) Freeing *Pseudomonas putida* KT2440 of its proviral load strengthens endurance to environmental stresses, *Environ. Microbiol. 17*, 76-90.

[22] Lieder, S., Nikel, P. I., de Lorenzo, V., and Takors, R. (2015) Genome reduction boosts heterologous gene expression in *Pseudomonas putida*, *Microb. Cell Fact. 14*, 23.

[23] Morimoto, T., Kadoya, R., Endo, K., Tohata, M., Sawada, K., Liu, S., Ozawa, T., Kodama, T., Kakeshita, H., Kageyama, Y., Manabe, K., Kanaya, S., Ara, K., Ozaki, K., and Ogasawara, N. (2008) Enhanced Recombinant Protein Productivity by Genome Reduction in *Bacillus subtilis*, *DNA Res. 15*, 73-81.

[24] Lee, J. H., Sung, B. H., Kim, M. S., Blattner, F. R., Yoon, B. H., Kim, J. H., and Kim, S. C. (2009) Metabolic engineering of a reduced-genome strain of *Escherichia coli* for L-threonine production, *Microb. Cell Fact 8*, 2.

[25] Panke, S., Witholt, B., Schmid, A., and Wubbolts, M. G. (1998) Towards a biocatalyst for (*S*)-styrene oxide production: characterization of the styrene degradation pathway of *Pseudomonas* sp. strain VLB120, *Appl. Environ. Microbiol. 64*, 2032-2043.

[26] Loeschcke, A., and Thies, S. (2015) *Pseudomonas putida* − a versatile host for the production of natural products, *Appl. Microbiol. Biotechnol. 99*, 6197-6214.

[27] Klein, A. S., Domröse, A., Bongen, P., Brass, H. U. C., Classen, T., Loeschcke, A., Drepper, T., Laraia, L., Sievers, S., Jaeger, K.-E., and Pietruszka, J. (2017) New prodigiosin derivatives obtained by mutasynthesis in *Pseudomonas putida*, *ACS Synth. Biol. 6*, 1757-1765.

[28] Tiso, T., Wierckx, N., and Blank, L. M. (2014) Non-pathogenic *Pseudomonas* as platform for industrial biocatalysis, In *Industrial Biocatalysis* (Grunwald, P., Ed.), pp 323-372, Pan Stanford.

[29] Heipieper, H. J., Neumann, G., Cornelissen, S., and Meinhardt, F. (2007) Solvent-tolerant bacteria for biotransformations in two-phase fermentation systems, *Appl. Microbiol. Biotechnol. 74*, 961-973.

[30] Blank, L. M., Ionidis, G., Ebert, B. E., Buhler, B., and Schmid, A. (2008) Metabolic response of *Pseudomonas putida* during redox biocatalysis in the presence of a second octanol phase, *FEBS J. 275*, 5173-5190.

[31] Park, J. B., Bühler, B., Panke, S., Witholt, B., and Schmid, A. (2007) Carbon metabolism and product inhibition determine the epoxidation efficiency of solvent-tolerant *Pseudomonas* sp. strain VLB120DeltaC, *Biotechnol. Bioeng. 98*, 1219-1229.

[32] Volmer, J., Schmid, A., and Buhler, B. (2017) The application of constitutively solvent-tolerant *P. taiwanensis* VLB120ΔCΔttgV for stereospecific epoxidation of toxic styrene alleviates carrier solvent use, *Biotechnol. J. 12*, 1600558.

[33] Lang, K., Zierow, J., Buehler, K., and Schmid, A. (2014) Metabolic engineering of *Pseudomonas* sp. strain VLB120 as platform biocatalyst for the production of isobutyric acid and other secondary metabolites, *Microb. Cell Fact. 13*, 2.

[34] Gross, R., Bühler, K., and Schmid, A. (2013) Engineered catalytic biofilms for continuous large scale production of *n*-octanol and (*S*)-styrene oxide, *Biotechnol. Bioeng. 110*, 424-436.

[35] Wynands, B., Lenzen, C., Otto, M., Koch, F., Blank, L. M., and Wierckx, N. (2018) Metabolic engineering of *Pseudomonas taiwanensis* VLB120 with minimal genomic modifications for high-yield phenol production, *Metab. Eng. 47*, 121-133.

[36] Köhler, K. A., Blank, L. M., Frick, O., and Schmid, A. (2015) D-Xylose assimilation via the Weimberg pathway by solvent-tolerant *Pseudomonas taiwanensis* VLB120, *Environ. Microbiol. 17*, 156-170.

[37] Macnab, R. M. (1996) Flagella and motility, In *Escherichia coli and Salmonella: Cellular and Molecular Biology* (C., N. F., R. Curtiss, R., III, Ingraham, J. L., Lin, E. C. C., Low, K. B., Magasanik, B., Reznikoff, W. S., Riley, M., Schaechter, M., and Umbarger, H. E., Eds.) 2 ed., pp 123-145, ASM Press, Washington D.C.

[38] Neidhart, F. C. (1987) Chemical composition of *Escherichia coli*, In *Escherichia coli and Salmonella typhimurium: Cellular and Molecular Biology* (C., N. F., Ingraham, J. L., Low, K. B., Magasanik, B., Schaechter, M., and Umbarger, H. E., Eds.), AMS Press, Washington D.C.
[39] Martinez-Garcia, E., Nikel, P. I., Chavarria, M., and de Lorenzo, V. (2014) The metabolic cost of flagellar motion in *Pseudomonas putida* KT2440, *Environ. Microbiol. 16*, 291-303.
[40] Martínez-García, E., and de Lorenzo, V. (2011) Engineering multiple genomic deletions in Gram-negative bacteria: analysis of the multi-resistant antibiotic profile of *Pseudomonas putida* KT2440, *Environ. Microbiol. 13*, 2702-2716.
[41] Domínguez-Cuevas, P., Gonzalez-Pastor, J. E., Marques, S., Ramos, J. L., and de Lorenzo, V. (2006) Transcriptional tradeoff between metabolic and stress-response programs in *Pseudomonas putida* KT2440 cells exposed to toluene, *J. Biol. Chem 281*, 11981-11991.
[42] Molina-Santiago, C., Udaondo, Z., Gomez-Lozano, M., Molin, S., and Ramos, J. L. (2017) Global transcriptional response of solvent-sensitive and solvent-tolerant *Pseudomonas putida* strains exposed to toluene, *Environ. Microbiol 19*, 645-658.
[43] Volkers, R. J., Ballerstedt, H., Ruijssenaars, H., de Bont, J. A., de Winde, J. H., and Wery, J. (2009) TrgI, toluene repressed gene I, a novel gene involved in toluene-tolerance in *Pseudomonas putida* S12, *Extremophiles. 13*, 283-297.
[44] Kieboom, J., Bruinenberg, R., Keizer-Gunnink, I., and de Bont, J. A. (2001) Transposon mutations in the flagella biosynthetic pathway of the solvent-tolerant *Pseudomonas putida* S12 result in a decreased expression of solvent efflux genes, *FEMS Microbiol. Lett 198*, 117-122.
[45] Segura, A., Duque, E., Hurtado, A., and Ramos, J. L. (2001) Mutations in genes involved in the flagellar export apparatus of the solvent-tolerant *Pseudomonas putida* DOT-T1E strain impair motility and lead to hypersensitivity to toluene shocks, *J. Bacteriol. 183*, 4127-4133.
[46] Belas, R. (2014) Biofilms, flagella, and mechanosensing of surfaces by bacteria, *Trends Microbiol. 22*, 517-527.
[47] Chawla, R., Ford, K. M., and Lele, P. P. (2017) Torque, but not FliL, regulates mechanosensitive flagellar motor-function, *Sci. Rep 7*, 5565.
[48] Partridge, J. D., Nieto, V., and Harshey, R. M. (2015) A new player at the flagellar motor: FliL controls both motor output and bias, *mBio 6*, e02367-02314.
[49] Guttenplan, S. B., and Kearns, D. B. (2013) Regulation of flagellar motility during biofilm formation, *FEMS Microbiol. Rev. 37*, 849-871.
[50] O'Toole, G. A. (2011) Microtiter dish biofilm formation assay, *J. Vis. Exp 47*, 2437.
[51] Rosche, B., Li, X. Z., Hauer, B., Schmid, A., and Bühler, K. (2009) Microbial biofilms: a concept for industrial catalysis?, *Trends Biotechnol. 27*, 636-643.
[52] Halan, B., Bühler, K., and Schmid, A. (2012) Biofilms as living catalysts in continuous chemical syntheses, *Trends Biotechnol. 30*, 453-465.
[53] Halan, B., Letzel, T., Schmid, A., and Buehler, K. (2014) Solid support membrane-aerated catalytic biofilm reactor for the continuous synthesis of (*S*)-styrene oxide at gram scale, *Biotechnol. J. 9*, 1339-1349.
[54] Gross, R., Lang, K., Bühler, K., and Schmid, A. (2010) Characterization of a biofilm membrane reactor and its prospects for fine chemical synthesis, *Biotechnol. Bioeng 105*, 705-717.
[55] Tolker-Nielsen, T., and Molin, S. (2004) The biofilm lifestyle of Pseudomonads, In *Pseudomonas: Volume 1 Genomics, Life Style and Molecular Architecture* (Ramos, J.-L., Ed.), pp 547-571, Springer US, Boston, MA.
[56] Martínez-Gil, M., Ramos-González, M. I., and Espinosa-Urgel, M. (2014) Roles of cyclic di-GMP and the Gac system in transcriptional control of the genes coding for the *Pseudomonas putida* adhesins LapA and LapF, *J. Bacteriol. 196*, 1484-1495.
[57] Boyd, C. D., Smith, T. J., El-Kirat-Chatel, S., Newell, P. D., Dufrene, Y. F., and O'Toole, G. A. (2014) Structural features of the *Pseudomonas fluorescens* biofilm adhesin LapA required for LapG-dependent cleavage, biofilm formation, and cell surface localization, *J. Bacteriol 196*, 2775-2788.
[58] Gjermansen, M., Nilsson, M., Yang, L., and Tolker-Nielsen, T. (2010) Characterization of starvation-induced dispersion in *Pseudomonas putida* biofilms: genetic elements and molecular mechanisms, *Mol. Microbiol 75*, 815-826.

[59] Lahesaare, A., Ainelo, H., Teppo, A., Kivisaar, M., Heipieper, H. J., and Teras, R. (2016) LapF and its regulation by fis affect the cell surface hydrophobicity of *Pseudomonas putida*, *PLoS One. 11*, e0166078.

[60] Rojas, A., Duque, E., Mosqueda, G., Golden, G., Hurtado, A., Ramos, J. L., and Segura, A. (2001) Three efflux pumps are required to provide efficient tolerance to toluene in *Pseudomonas putida* DOT-T1E, *J. Bacteriol 183*, 3967-3973.

[61] Volmer, J., Neumann, C., Bühler, B., and Schmid, A. (2014) Engineering of *Pseudomonas taiwanensis* VLB120 for constitutive solvent tolerance and increased specific styrene epoxidation activity, *Appl. Environ. Microbiol. 80*, 6539-6548.

[62] Ramos-Gonzalez, M. I., Duque, E., and Ramos, J. L. (1991) Conjugational transfer of recombinant DNA in cultures and in soils: host range of Pseudomonas putida TOL plasmids, *Appl. Environ. Microbiol. 57*, 3020-3027.

[63] Zobel, S., Benedetti, I., Eisenbach, L., de Lorenzo, V., Wierckx, N., and Blank, L. M. (2015) Tn7-based device for calibrated heterologous gene expression in *Pseudomonas putida*, *ACS Synth. Biol. 4*, 1341-1351.

[64] Bruder, S., Reifenrath, M., Thomik, T., Boles, E., and Herzog, K. (2016) Parallelised online biomass monitoring in shake flasks enables efficient strain and carbon source dependent growth characterisation of *Saccharomyces cerevisiae*, *Microb. Cell Fact. 15*, 127.

[65] Köhler, K. A., Ruckert, C., Schatschneider, S., Vorholter, F. J., Szczepanowski, R., Blank, L. M., Niehaus, K., Goesmann, A., Puhler, A., Kalinowski, J., and Schmid, A. (2013) Complete genome sequence of *Pseudomonas* sp. strain VLB120 a solvent tolerant, styrene degrading bacterium, isolated from forest soil, *J. Biotechnol. 168*, 729-730.

[66] Kjeldsen, K. R., and Nielsen, J. (2009) In silico genome-scale reconstruction and validation of the *Corynebacterium glutamicum* metabolic network, *Biotechnol. Bioeng 102*, 583-597.

[67] Martinez-Gil, M., Yousef-Coronado, F., and Espinosa-Urgel, M. (2010) LapF, the second largest *Pseudomonas putida* protein, contributes to plant root colonization and determines biofilm architecture, *Mol. Microbiol. 77*, 549-561.

[68] Dziewit, L., and Radlinska, M. (2016) Two inducible prophages of an antarctic *Pseudomonas* sp. ANT_H14 use the same capsid for packaging their genomes – characterization of a novel phage helper-satellite system, *PLoS One. 11*, e0158889.

[69] Casjens, S. (2003) Prophages and bacterial genomics: what have we learned so far?, *Mol. Microbiol 49*, 277-300.

[70] Arndt, D., Grant, J. R., Marcu, A., Sajed, T., Pon, A., Liang, Y., and Wishart, D. S. (2016) PHASTER: a better, faster version of the PHAST phage search tool, *Nucleic Acids Res. 44*, W16-21.

[71] Rojas, A., Segura, A., Guazzaroni, M. E., Teran, W., Hurtado, A., Gallegos, M. T., and Ramos, J. L. (2003) *In vivo* and *in vitro* evidence that TtgV is the specific regulator of the TtgGHI multidrug and solvent efflux pump of *Pseudomonas putida*, *J. Bacteriol 185*, 4755-4763.

[72] Sangster, J. (1989) Octanol-water partition coefficients of simple organic compounds, *J. Phys. Chem. Ref. Data 18*, 1111-1229.

[73] Roma-Rodrigues, C., Santos, P. M., Benndorf, D., Rapp, E., and Sá-Correia, I. (2010) Response of *Pseudomonas putida* KT2440 to phenol at the level of membrane proteome, *J. Proteomics 73*, 1461-1478.

[74] Putrinš, M., Ilves, H., Lilje, L., Kivisaar, M., and Hõrak, R. (2010) The impact of ColRS two-component system and TtgABC efflux pump on phenol tolerance of *Pseudomonas putida* becomes evident only in growing bacteria, *BMC Microbiol. 10*, 110-110.

[75] Wierckx, N. J. P., Ballerstedt, H., de Bont, J. A. M., and Wery, J. (2005) Engineering of solvent-tolerant *Pseudomonas putida* S12 for bioproduction of phenol from glucose, *Appl. Environ. Microbiol. 71*, 8221-8227.

[76] Kivistik, P. A., Putrinš, M., Püvi, K., Ilves, H., Kivisaar, M., and Hõrak, R. (2006) The ColRS two-component system regulates membrane functions and protects *Pseudomonas putida* against phenol, *J. Bacteriol. 188*, 8109-8117.

[77] Hartmans, S., Smits, J. P., van der Werf, M. J., Volkering, F., and de Bont, J. A. M. (1989) Metabolism of styrene oxide and 2-phenyl ethanol in the styrene degrading *Xanthobacter* strain 124X, *Appl. Environ. Microbiol. 55*, 2850-2855.

[78] Duetz, W. A., Ruedi, L., Hermann, R., O'Connor, K., Buchs, J., and Witholt, B. (2000) Methods for intense aeration, growth, storage, and replication of bacterial strains in microtiter plates, *Appl. Environ. Microbiol. 66*, 2641-2646.

[79] Gibson, D. G., Young, L., Chuang, R.-Y., Venter, J. C., Hutchison Iii, C. A., and Smith, H. O. (2009) Enzymatic assembly of DNA molecules up to several hundred kilobases, *Nat. Methods 6*, 343.

[80] Chomczynski, P., and Rymaszewski, M. (2006) Alkaline polyethylene glycol-based method for direct PCR from bacteria, eukaryotic tissue samples, and whole blood, *BioTechniques 40*, 454-458.

[81] Martínez-García, E., and Lorenzo, V. (2011) Engineering multiple genomic deletions in Gram-negative bacteria: analysis of the multi-resistant antibiotic profile of *Pseudomonas putida* KT2440, *Environ Microbiol 13*.

[82] Hanahan, D. (1985) Techniques for transformation of *E. coli*., In *DNA Cloning: A Practical Approach* (Glover, D. M., Ed.), pp 109-135, IRL Press, Oxford.

[83] de Lorenzo, V., and Timmis, K. N. (1994) Analysis and construction of stable phenotypes in Gram-negative bacteria with Tn5- and Tn10-derived minitransposons., *Methods Enzymol 235*, 386-405.

[84] Ditta, G., Stanfield, S., Corbin, D., and Helinski, D. R. (1980) Broad host range DNA cloning system for Gram-negative bacteria: construction of a gene bank of *Rhizobium meliloti*, *Proc. Natl. Acad. Sci. U.S.A. 77*, 7347-7351.

Supplemental information

Table of contents

Table S1. Genetic organization of the flagellar cluster. Listed are the genes of *P. taiwanensis* VLB120's flagellar cluster with their respective locus tag, name, and description of the encoded protein. Moreover, the deletion regions denoted as flag1 and flag2 and the segment in-between the deleted fragments are indicated. Base pair positions refer to accession number CP003961.1.

Region	Gene locus tag	Gene name	Description
flag1 (3767793-3812598 bp)	PVLB_17040	-	hypothetical protein (shows homology to FliK)
	PVLB_17045	-	hypothetical protein (FlhB domain-containing protein)
	PVLB_17050	-	hypothetical protein
	PVLB_17055	-	hypothetical protein
	PVLB_17060	*cheW*	Purine-binding chemotaxis protein CheW
	PVLB_17065	-	hypothetical protein (shows homology to CheW)
	PVLB_17070	-	ParA family ATPase
	PVLB_17075	*motD*	flagellar motor protein MotD
	PVLB_17080	*motC*	flagellar motor protein MotC
	PVLB_17085	*cheAB*	chemotaxis response regulator protein-glutamate methylesterase
	PVLB_17090	*cheA*	chemotaxis signal transduction histidine kinase CheA
	PVLB_17095	*cheZ*	chemotaxis phosphatase CheZ
	PVLB_17100	*cheY*	response regulator receiver protein
	PVLB_17105	*fliA*	RNA polymerase sigma 28 factor FliA (flagellar biosynthesis sigma factor)
	PVLB_17110	*fleN*	flagellar number regulator FleN
	PVLB_17115	*flhF*	flagellar biosynthesis regulator FlhF
	PVLB_17120	*flhA*	flagellar biosynthesis protein FlhA
	PVLB_17125	*flhB*	flagellar biosynthesis protein FlhB
	PVLB_17130	*fliR*	flagellar biosynthesis protein FliR
	PVLB_17135	*fliQ*	flagellar biosynthesis protein FliQ
	PVLB_17140	*fliP*	flagellar biosynthesis protein FliP
	PVLB_17145	*fliO*	flagellar protein FliO
	PVLB_17150	*fliN*	flagellar motor switch protein FliN
	PVLB_17155	*fliM*	flagellar motor switch protein FliM
	PVLB_17160	*fliL*	flagellar basal body-associatged protein FliL
	PVLB_17165	*fliK*	flagellar hook-length control protein FliK
	PVLB_17170	-	Htp protein
	PVLB_17175	-	CheY-like response regulator receiver protein
	PVLB_17180	-	anti-sigma F factor antagonist
	PVLB_17185	*fliJ*	flagellar biosynthesis chaperone
	PVLB_17190	*fliI*	flagellum-specific ATP synthase
	PVLB_17195	*fliH*	flagellar assembly protein FliH
	PVLB_17200	*fliG*	flagellar motor switch protein FliG
	PVLB_17205	*fliF*	flagellar MS-ring protein FliF
	PVLB_17210	*fliE*	flagellar hook-basal body protein FliE
	PVLB_17215	*fleR*	sigma-54-dependent Fis family transcriptional regulator FleR
	PVLB_17220	*fleS*	PAS/PAC sensor signal transduction histidine kinase FleS
	PVLB_17225	*fleQ*	transcriptional regulator FleQ

Table S1 (continued)

Region	Gene locus tag	Gene name	Description
flag1 (3767793-3812598 bp)	PVLB_17230	*fliT*	flagellar protein FliT
	PVLB_17235	*fliS*	flagellain-specific chaperone FliS
	PVLB_17240	*fliD*	flagellar filament capping protein FliD
	PVLB_17245	*flaG*	flagellar protein FlaG
	PVLB_17250	*fliC*	flagellin FliC
	PVLB_17255	-	hypothetical protein
	PVLB_17260	-	hypothetical protein
flagella-unrelated island	PVLB_17265	-	3-oxoacyl-ACP synthase
	PVLB_17270	-	N-acylneuraminate-9-phosphate synthase
	PVLB_17275	-	N-acetyltransferase GCN5
	PVLB_17280	-	N-acylneuraminate cytidylyltransferase
	PVLB_17285	-	DegT/DnrJ/EryC1/StrS aminotransferase
	PVLB_17290	-	polysaccharide biosynthesis protein CapD
	PVLB_17295	-	glycosyl transferase family protein
	PVLB_17300	-	cephalosporin hydroxylase
	PVLB_17305	-	type 11 methyltransferase
	PVLB_17310	-	NAD-dependent epimerase/dehydratase
	PVLB_17315	-	C-methyltransferase
	PVLB_17320	-	dTDP-4-dehydrorhamnose 3,5-epimerase
	PVLB_17325	-	CDP-glucose 4,6-dehydratase
	PVLB_17330	-	glucose-1-phosphate cytidylyltransferase
	PVLB_17335	-	glycosyl transferase family protein
flag2 (3832716-3849243 bp)	PVLB_17340	*flgL*	flagellar hook-associated protein FlgL
	PVLB_17345	*flgK*	flagellar hook-associated protein FlgK
	PVLB_17350	*flgJ*	flagellar rod assembly protein/muramidase FlgJ
	PVLB_17355	*flgI*	flagellar basal-body P-ring protein FlgI
	PVLB_17360	*flgH*	flagellar basal body L-ring protein FlgH
	PVLB_17365	*flgG*	flagellar basal body rod protein FlgG
	PVLB_17370	*flgF*	flagellar basal body rod protein FlgF
	PVLB_17375	-	hypothetical protein
	PVLB_17380	*flgE*	flagellar hook protein FlgE
	PVLB_17385	*flgD*	flagellar basal body rod modification protein FlgD
	PVLB_17390	*flgC*	flagellar basal body rod protein FlgC
	PVLB_17395	*flgB*	flagellar basal body rod protein FlgB
	PVLB_17400	*cheR*	CheR-type MCP methyltransferase (chemotaxis protein)
	PVLB_17405	*cheV*	chemotaxis protein CheV
	PVLB_17410	*flgA*	flagellar basal body P-ring biosynthesis protein FlgA
	PVLB_17415	*flgM*	anti-sigma-28 factor FlgM
	PVLB_17420	*flgN*	flagella synthesis protein FlgN
	PVLB_17425	-	type IV pilus assembly PilZ (flagellar brake protein)

Table S2. Genetic organization of the *lap* clusters. Listed are the denoted *lap* regions of *P. taiwanensis* VLB120 and the included genes with their locus tag, name, and description. Base pair positions refer to accession number CP003961.1.

Region	Gene locus tag	Gene name	Description
lap1 (204010-223295 bp)	PVLB_00915	*lapG*	periplasmatic cysteine protease LapG
	PVLB_00920	*lapD*	diguanylate cyclase/phosphodiesterase
	PVLB_00925	-	hypothetical protein
	PVLB_00930	*lapA*	large adhesive protein LapA
	PVLB_00935	*lapB*	type I secretion system permease/ATPase (LapA exporter ATPase component)
	PVLB_00940	*lapC*	HlyD family type I secretion membrane fusion protein (LapA exporter membrane protein component)
lap2 (3918406-3933516 bp)	PVLB_17755	-	outer membrane adhesin-like protein (shows homology to LapA)
	PVLB_17760	*lapE*	type I secretion system ATPase LapE (annotated as TolC)
	PVLB_17765	-	type I secretion system ATPase (shows homology to LapB)
	PVLB_17770	-	HlyD family type I secretion membrane fusion protein (shows homology to LapC)
	PVLB_17775	-	hypothetical protein
	PVLB_17780	-	DTW domain-containing protein
	PVLB_17785	-	HlyD family type I secretion membrane fusion protein (shows homology to LapC)
lap3 (4601770-4618483 bp)	not available	*lapF*	large adhesive protein LapF (ORF: 4601818-4612590 bp)
	PVLB_20970	*lapH*	TolC family type I secretion outer membrane protein
	PVLB_20975	*lapI*	ABC transporter
	PVLB_20980	*lapJ*	HlyD family type I secretion membrane fusion protein
	PVLB_20985	-	CheW-like chemotaxis signal transduction protein

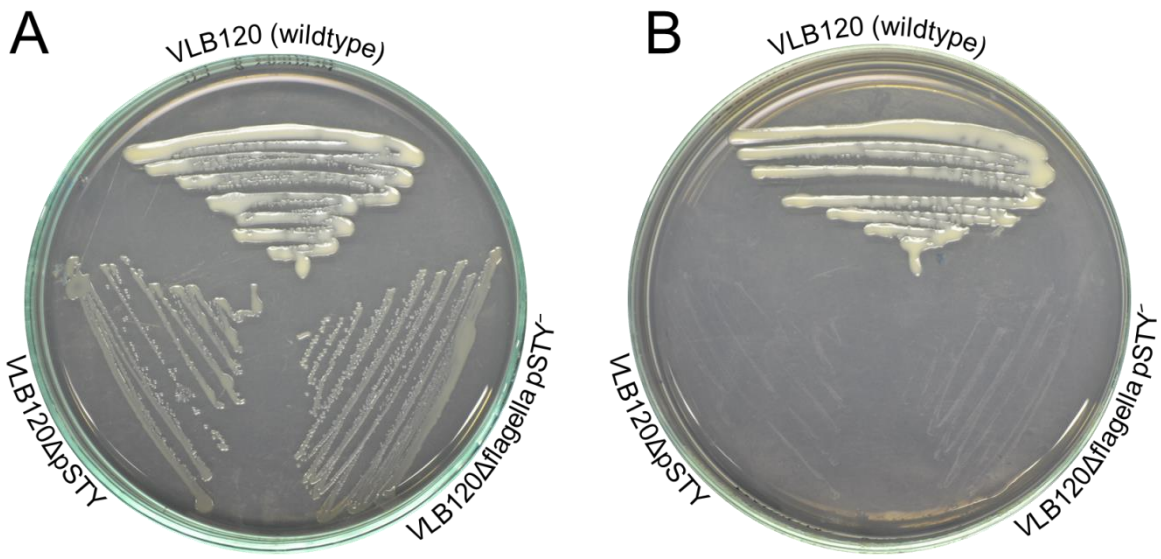

Figure S1. Growth in a styrene-saturated vapor phase. Growth of *Pseudomonas taiwanensis* VLB120 (wildtype), VLB120ΔpSTY, and VLB120Δflagella pSTY$^-$ in a styrene vapor phase on mineral salt medium with 20 mM glucose (A) and without an additional carbon source (B). Pictures were taken after an incubation of 72 h at room temperature.

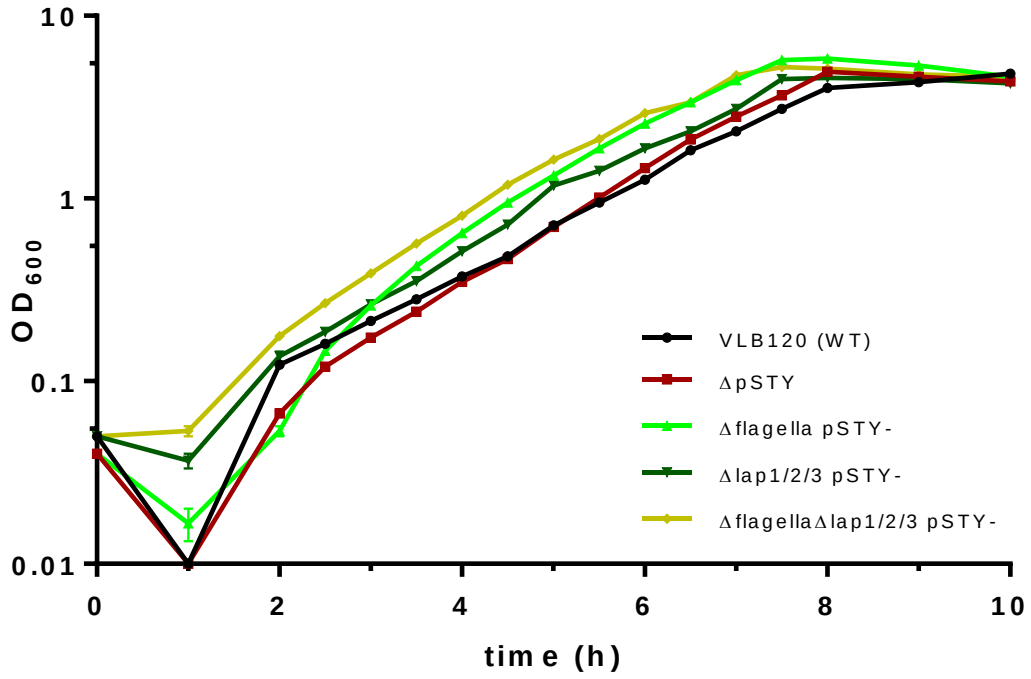

Figure S2. Growth kinetics of various streamlined strains on a logarithmic scale. Shown are the growth kinetics of *P. taiwanensis* VLB120 (wildtype), VLB120ΔpSTY, VLB120Δflagella pSTY$^-$, VLB120Δlap1/2/3 pSTY$^-$, and VLB120ΔflagellaΔlap1/2/3 pSTY$^-$ obtained from a growth experiment with the manually measured OD_{600} values from Fig. 5A on a logarithmic scale.

Table S3. Proviral DNA segments of *P. taiwanensis* VLB120. Shown are the proviral regions of *P. taiwanensis* VLB120 with their size and position as they were detected by the PHASTER online tool(Arndt et al., 2016) and as they were deleted. Base pair positions refer to accession number CP003961.1. Prophage region 1 and 2 were combined to only one region as the predicted sequences overlap. The completeness is given as predicted by PHASTER. A more detailed overview of the five proviral segments is given in Table S4.

Region	Region length (kb)	Region position (bp)	Completeness	Deleted region length (kb)	Deleted region position (bp)
prophage 1/2	113.3	2017944-2131212	intact/questionable	105.6	2025574-2131212
prophage 3	52.9	4109034-4161947	intact	46.3	4115506-4161797
prophage 4	12.6	4568464-4581079	incomplete	12.4	4568696-4581079
prophage 5	47.1	5267515-5314593	intact	41.9	5268120-5310003

The prophages were not fully erased as they were predicted by PHASTER because they harbor CDS involved in important physiological functions (e.g., tRNA- and ribosomal protein-coding sequences). The deletion region was chosen after a manual evaluation on the genes lying within the predicted prophagic sequence.

Table S4. Detailed overview of the proviral segments. Shown are detailed information on the prophages. This table is adapted from a PHASTER analysis(Arndt et al., 2016) of the genome of *P. taiwanensis* VLB120 (accession number: CP003961.1). No prophages were predicted to be on the megaplasmid pSTY. Genes that are localized between the attachment sites but were not listed by PHASTER were manually added. Sequences with grayed backgrounds were not deleted.

Region	Gene locus tag	Sequence name	Description	Hits against virus and prophage database
prophage 1	-	*attL*	left attachment site (2017944-2017955 bp)	no
	PVLB_08885	*thrS*	threonyl-tRNA ligase	n.a.
	PVLB_08890	*infC*	translation initiation factor IF-3	n.a.
	PVLB_08895	*rpmI*	50S ribosomal protein L35	n.a.
	PVLB_08900	*rplT*	50S ribosomal protein L20	n.a.
	PVLB_08905	*pheS*	phenylalanyl-tRNA ligase subunit α	n.a.
	PVLB_08910	*pheT*	phenylalanyl-tRNA ligase subunit β	n.a.
	PVLB_08915	*ihfA*	integration host factor subunit α	yes
	PVLB_08920	-	MerR family transcriptional regulator	no
	PVLB_t25826	-	tRNA-Pro	no
	PVLB_08925	-	integrase family protein	yes
	PVLB_08930	-	hypothetical protein	no
	PVLB_08935	-	hypothetical protein	no
	PVLB_08940	-	phosphoprotein phosphatase	yes

Table S4 (continued)

Region	Gene locus tag	Sequence name	Description	Hits against virus and prophage database
prophage 1	PVLB_08945	-	hypothetical protein	yes
	PVLB_08950	-	hypothetical protein	no
	PVLB_08955	-	hypothetical protein	yes
	PVLB_08960	-	hypothetical protein	no
	PVLB_08965	-	hypothetical protein	no
	PVLB_08970	-	putative transcriptional regulator	no
	PVLB_08975	-	hypothetical protein	no
	PVLB_08980	-	hypothetical protein	yes
	PVLB_08985	-	hypothetical protein	no
	PVLB_08990	-	hypothetical protein	yes
	PVLB_08995	-	hypothetical protein	no
	PVLB_09000	-	ssDNA-binding protein	yes
	PVLB_09005	-	hypothetical protein	no
	PVLB_09010	-	LuxR family transcriptional regulator	yes
	PVLB_09015	-	hypothetical protein	yes
	PVLB_09020	-	hypothetical protein (putative tellurite resistance protein)	yes
	PVLB_09025	-	putative transcriptional regulator	yes
	PVLB_09030	-	phage regulatory protein	yes
	PVLB_09035	-	hypothetical protein	no
	PVLB_09040	-	phage replication protein	yes
	PVLB_09045	-	replicative DNA helicase	yes
	PVLB_09050	-	hypothetical protein	no
	PVLB_09055	-	hypothetical protein	yes
	PVLB_09060	-	hypothetical protein	yes
	PVLB_09065	-	phage integrase family protein	yes
	PVLB_09070	-	hypothetical protein	no
	PVLB_09075	-	hypothetical protein	yes
	PVLB_09080	-	hypothetical protein	no
	PVLB_09085	-	phage holin	yes
	PVLB_09090	-	hypothetical protein	no
	PVLB_09095	-	hypothetical protein	no
	PVLB_09100	-	phage holin	yes
	PVLB_09105	-	P27 family phage terminase small subunit	yes
	PVLB_09110	-	phage terminase-like protein	yes
	PVLB_09115	-	putative phage portal protein, HK97 family	yes
	PVLB_09120	-	peptidase S14 ClpP	yes
	PVLB_09125	-	phage major capsid protein, HK97 family	yes
	PVLB_09130	-	hypothetical protein	yes
	PVLB_09135	-	hypothetical protein	yes
	PVLB_09140	-	phage head-tail adaptor	yes
	PVLB_09145	-	HK97 family phage protein	yes
	PVLB_09150	-	hypothetical protein	yes
	PVLB_09155	-	hypothetical protein	no
	-	*attL*	left attachment site (2052053-2052064 bp)	no
	PVLB_09160	-	hypothetical protein	yes
	PVLB_09165	-	hypothetical protein	yes

Table S4 (continued)

Region	Gene locus tag	Sequence name	Description	Hits against virus and prophage database
prophage 1	PVLB_09170	-	hypothetical protein	no
	PVLB_09175	-	hypothetical protein	yes
	PVLB_09180	-	lambda family phage tail tape measure protein	yes
	PVLB_09185	-	phage minor tail family protein	yes
	PVLB_09190	-	lambda-like phage minor tail protein L	yes
	PVLB_09195	-	hypothetical protein	yes
	PVLB_09200	-	phage tail assembly protein	yes
	PVLB_09205	-	phage host specificity protein	yes
	PVLB_09210	-	hypothetical protein	yes
	PVLB_09215	-	hypothetical protein	yes
	PVLB_09220	-	tail fiber assembly domain protein	yes
	PVLB_09225	-	hypothetical protein	yes
	PVLB_09230	-	hypothetical protein	yes
	PVLB_09235	-	hypothetical protein	no
	PVLB_09240	-	hypothetical protein	no
	PVLB_09245	-	hypothetical protein	no
	PVLB_09250	-	integrase family protein	yes
	PVLB_09255	-	hypothetical protein	no
	PVLB_09260	-	phosphoprotein phosphatase	yes
	PVLB_09265	-	hypothetical protein	yes
	PVLB_09270	-	hypothetical protein	no
	PVLB_09275	-	hypothetical protein	yes
	PVLB_09280	-	hypothetical protein	no
	PVLB_09285	-	hypothetical protein	yes
	PVLB_09290	-	hypothetical protein	no
	PVLB_09295	-	hypothetical protein	no
	PVLB_09300	-	hypothetical protein	yes
	PVLB_09305	-	hypothetical protein	no
	PVLB_09310	-	hypothetical protein	no
	PVLB_09315	-	hypothetical protein	yes
	PVLB_09320	-	homing nuclease	yes
	PVLB_09325	-	hypothetical protein (protein chain release factor B)	no
	PVLB_09330	-	siphovirus Gp157 family protein	yes
	PVLB_09335	-	hypothetical protein	yes
	PVLB_09340	-	hypothetical protein	no
	PVLB_09345	-	hypothetical protein	no
	PVLB_09350	-	hypothetical protein	no
	PVLB_09355	-	hypothetical protein	yes
	PVLB_09360	-	hypothetical protein	no
	PVLB_09365	-	hypothetical protein	no
	PVLB_09370	-	hypothetical protein	no
	PVLB_09375	-	bacteriophage protein	yes
	PVLB_09380	-	hypothetical protein	no
	PVLB_09385	-	hypothetical protein	yes
	PVLB_09390	-	hypothetical protein	yes
	PVLB_09395	-	hypothetical protein	no

Table S4 (continued)

Region	Gene locus tag	Sequence name	Description	Hits against virus and prophage database
prophage 1	PVLB_09400	-	hypothetical protein	no
	PVLB_09405	-	hypothetical protein	no
	PVLB_09410	-	prophage PSPPH03, Cro/CI family transcriptional regulator	no
	PVLB_09415	-	regulatory protein cro	yes
	PVLB_09420	-	hypothetical protein	yes
	PVLB_09425	-	hypothetical protein	yes
	PVLB_09430	-	phage-encoded protein	yes
	PVLB_09435	-	hypothetical protein	yes
	PVLB_09440	-	IstB ATP binding domain-containing protein	yes
	PVLB_09445	-	hypothetical protein	yes
	PVLB_09450	-	hypothetical protein	no
	PVLB_09455	-	hypothetical protein	yes
	PVLB_09460	-	hypothetical protein	yes
	PVLB_09465	-	NinB family protein	yes
	PVLB_09470	-	bacteriophage lambda NinG family protein	yes
	PVLB_09475	-	hypothetical protein (ATP-dependent DNA ligase)	yes
	PVLB_09480	-	hypothetical protein	no
	PVLB_09485	-	hypothetical protein	no
	PVLB_09490	-	hypothetical protein	yes
	PVLB_09495	-	hypothetical protein	yes
	PVLB_09500	-	hypothetical protein	no
	PVLB_09505	-	hypothetical protein	no
	PVLB_09510	-	hypothetical protein	yes
	PVLB_09515	-	hypothetical protein (uncharacterized conserved protein)	yes
	PVLB_09520	-	phage terminase protein	yes
	PVLB_09535	-	hypothetical protein	yes
	PVLB_09540	-	hypothetical protein	yes
	PVLB_09545	-	hypothetical protein	yes
	PVLB_09550	-	hypothetical protein	no
	PVLB_09555	-	hypothetical protein	yes
	PVLB_09560	-	hypothetical protein	yes
	PVLB_09565	-	hypothetical protein	yes
	PVLB_09570	-	hypothetical protein	yes
	PVLB_09575	-	tail protein 3	yes
	PVLB_09580	-	hypothetical protein	yes
	PVLB_09585	-	hypothetical protein	yes
	PVLB_09590	-	Phage tail tape measure protein lambda	yes
	PVLB_09595	-	Phage minor tail	yes
	PVLB_09600	-	phage minor tail protein L	yes
	PVLB_09605	-	NLP/P60 protein	yes
	PVLB_09610	-	hypothetical protein	n.a.
	PVLB_09615	-	hypothetical protein	n.a.
	PVLB_09620	-	hypothetical protein	n.a.
	PVLB_09625	-	hypothetical protein	n.a.
	PVLB_09630	-	hypothetical protein	n.a.

Table S4 (continued)

Region	Gene locus tag	Sequence name	Description	Hits against virus and prophage database
prophage 1	PVLB_09635	-	hypothetical protein (signal recognition particle GTPase)	yes
	PVLB_09640	-	bacteriophage lambda tail assembly I	yes
	PVLB_09645	-	phage host specificity protein	yes
	PVLB_09650	-	hypothetical protein (Asp-tRNAAsn/Glu-tRNAGln amidotransferase B subunit)	yes
	PVLB_09655	-	hypothetical protein	no
	PVLB_09660	-	hypothetical protein	yes
	PVLB_09665	-	tail fiber assembly domain protein	yes
	PVLB_09670	-	hypothetical protein	yes
	PVLB_09675	-	hypothetical protein	yes
	PVLB_09680	-	hypothetical protein	no
	PVLB_09685	-	hypothetical protein	no
	PVLB_09690	-	hypothetical protein	no
	-	*attR*	right attachment site (2109568-2109579 bp)	no
	-	*attR*	right attachment site (2121133-2121144 bp)	no
prophage 2	-	*attL*	left attachment site (2096902-2096913 bp)	no
	PVLB_09535	-	hypothetical protein	yes
	PVLB_09540	-	hypothetical protein	yes
	PVLB_09545	-	hypothetical protein	yes
	PVLB_09550	-	hypothetical protein	no
	PVLB_09555	-	hypothetical protein	yes
	PVLB_09560	-	hypothetical protein	yes
	PVLB_09565	-	hypothetical protein	yes
	PVLB_09570	-	hypothetical protein	yes
	PVLB_09575	-	tail protein 3	yes
	PVLB_09580	-	hypothetical protein	yes
	PVLB_09585	-	hypothetical protein (Trypsin-like serine proteases, typically periplasmic, contain C-terminal PDZ domain)	yes
	PVLB_09590	-	Phage tail tape measure protein lambda	yes
	PVLB_09595	-	Phage minor tail	yes
	PVLB_09600	-	phage minor tail protein L	yes
	PVLB_09605	-	NLP/P60 protein	yes
	PVLB_09610	-	hypothetical protein	n.a.
	PVLB_09615	-	hypothetical protein	n.a.
	PVLB_09620	-	hypothetical protein	n.a.
	PVLB_09625	-	hypothetical protein	n.a.
	PVLB_09630	-	hypothetical protein	n.a.
	PVLB_09635	-	hypothetical protein (signal recognition particle GTPase)	yes
	PVLB_09640	-	bacteriophage lambda tail assembly I	yes
	PVLB_09645	-	phage host specificity protein	yes
	PVLB_09650	-	hypothetical protein (Asp-tRNAAsn/Glu-tRNAGln amidotransferase B subunit)	yes
	PVLB_09655	-	hypothetical protein	no
	PVLB_09660	-	hypothetical protein	yes

Table S4 (continued)

Region	Gene locus tag	Sequence name	Description	Hits against virus and prophage database
prophage 2	PVLB_09665	-	tail fiber assembly domain protein	yes
	PVLB_09670	-	hypothetical protein	yes
	PVLB_09675	-	hypothetical protein	yes
	PVLB_09680	-	hypothetical protein	no
	PVLB_09685	-	hypothetical protein	no
	PVLB_09690	-	hypothetical protein	no
	PVLB_09695	-	ISPsy20, transposase IstB	yes
	PVLB_09700	-	ISPsy20, transposase IstA	yes
	PVLB_09705	-	phage integrase	no
	PVLB_09710	-	permease, MFS family protein	n.a.
	PVLB_09715	-	transcriptional regulator, IclR family protein	n.a.
	PVLB_09720	-	LysR family transcriptional regulator	n.a.
	PVLB_09725	-	hypothetical protein	n.a.
	PVLB_09730	-	nodulation protein d1	n.a.
	PVLB_09735	-	glyoxalase family protein	n.a.
	PVLB_09740	-	2Fe-2S) ferredoxin	n.a.
	-	*attR*	right attachment site (2131212-2131223 bp)	no
prophage 3	-	*attL*	left attachment site (4109034-4109045 bp)	n.a.
	PVLB_18615	-	GTP cyclohydrolase I	n.a.
	PVLB_18620	-	putative thiol-disulfide oxidoreductase DCC	n.a.
	PVLB_18625	-	site-specific recombinase, phage integrase family protein	n.a.
	PVLB_18630	-	hypothetical protein	n.a.
	PVLB_18635	-	plasmid replication protein	n.a.
	PVLB_18640	-	hypothetical protein	n.a.
	PVLB_18645	-	hypothetical protein (dTDP-D-glucose 4,6-dehydratase)	n.a.
	PVLB_18650	-	hypothetical protein	n.a.
	PVLB_18655	-	hypothetical protein	yes
	PVLB_18660	-	hypothetical protein	yes
	PVLB_18665	-	tail fiber assembly domain protein	yes
	PVLB_18670	-	hypothetical protein	yes
	PVLB_18675	-	hypothetical protein	no
	PVLB_18680	-	hypothetical protein (Asp-tRNAAsn/Glu-tRNAGln amidotransferase B subunit)	yes
	PVLB_18685	-	phage host specificity protein	yes
	PVLB_18690	-	phage GP20-like protein	yes
	PVLB_18695	-	lipoprotein	no
	PVLB_18700	-	tail assembly protein K	yes
	PVLB_18705	-	phage minor tail protein L	yes
	PVLB_18710	-	prophage LambdaSo, minor tail protein M	yes
	PVLB_18715	-	lambda family phage tail tape measure protein	yes
	PVLB_18720	-	hypothetical protein	yes
	PVLB_18725	-	hypothetical protein	yes
	PVLB_18730	-	phage major tail protein	yes
	PVLB_18735	-	hypothetical protein	no

Table S4 (continued)

Region	Gene locus tag	Sequence name	Description	Hits against virus and prophage database
prophage 3	PVLB_18740	-	hypothetical protein (NAD-dependent aldehyde dehydrogenases)	yes
	PVLB_18745	-	HK97 family phage protein	yes
	PVLB_18750	-	phage head-tail adaptor	yes
	PVLB_18755	-	hypothetical protein	yes
	PVLB_18760	-	hypothetical protein	no
	PVLB_18765	-	HK97 family phage major capsid protein	yes
	PVLB_18770	-	head maturation protease	yes
	PVLB_18775	-	HK97 family phage portal protein	yes
	PVLB_18780	-	hypothetical protein	yes
	PVLB_18785	-	terminase	yes
	PVLB_18790	-	hypothetical protein	yes
	PVLB_18795	-	phage holin	yes
	PVLB_18800	-	hypothetical protein	no
	PVLB_18805	-	putative lipoprotein	yes
	PVLB_18810	-	hypothetical protein	yes
	PVLB_18815	-	hypothetical protein	no
	PVLB_18820	-	hypothetical protein	no
	PVLB_18825	-	hypothetical protein	no
	PVLB_18830	-	hypothetical protein	yes
	PVLB_18835	-	hypothetical protein	yes
	PVLB_18840	-	DnaB domain-containing protein	yes
	PVLB_18845	-	IstB ATP binding domain-containing protein	yes
	PVLB_18850	-	hypothetical protein	yes
	PVLB_18855	-	hypothetical protein	yes
	PVLB_18860	-	hypothetical protein	yes
	PVLB_18865	-	hypothetical protein	yes
	PVLB_18870	-	hypothetical protein	yes
	PVLB_18875	-	hypothetical protein	no
	PVLB_18880	-	hypothetical protein	yes
	PVLB_18885	-	regulatory protein cro	yes
	PVLB_18890	-	cI repressor protein	yes
	PVLB_18895	-	LuxR family transcriptional regulator	yes
	PVLB_18900	-	carbon storage regulator	yes
	PVLB_18905	-	hypothetical protein	yes
	PVLB_18910	-	hypothetical protein	no
	PVLB_18915	-	hypothetical protein	no
	PVLB_18920	-	hypothetical protein	no
	PVLB_18925	-	hypothetical protein	yes
	PVLB_18930	-	hypothetical protein	no
	PVLB_18935	-	hypothetical protein (ABC-type antimicrobial peptide transport system, ATPase component)	no
	PVLB_18940	-	integrase family protein	yes
	PVLB_t25852	-	tRNA-Ser	n.d.
	-	*attR*	right attachment site (4161947-4161958 bp)	no

Table S4 (continued)

Region	Gene locus tag	Sequence name	Description	Hits against virus and prophage database
prophage 4	-	*attL*	left attachment site (4568464-4568482 bp)	no
	PVLB_t25860	-	tRNA-Leu	n.a.
	PVLB_20780	-	integrase family protein	yes
	PVLB_20785	-	hypothetical protein	no
	PVLB_20790	-	prophage CP4-57 regulatory protein	yes
	PVLB_20795	-	hypothetical protein	no
	PVLB_20800	-	hypothetical protein	no
	PVLB_20805	-	virulence-associated protein E	yes
	PVLB_20810	-	hypothetical protein (RecA-family ATPase)	yes
	PVLB_20815	-	hypothetical protein	no
	PVLB_20820	-	putative phage-like protein	yes
	PVLB_20825	-	HK97 family phage prohead protease	yes
	PVLB_20830	-	HK97 family phage portal protein	yes
	PVLB_20835	-	HNH endonuclease	yes
	PVLB_20840	-	TerS protein	yes
	PVLB_20845	-	phage terminase, large subunit	yes
	PVLB_20850	-	hypothetical protein	yes
	PVLB_20855	-	phage head-tail adaptor	yes
	-	*attR*	right attachment site (4580450-4581079 bp)	no
	PVLB_20860	-	hypothetical protein	yes
prophage 5	-	*attL*	left attachment site (5267515-5267564 bp)	no
	PVLB_23910	-	hypothetical protein	n.a.
	PVLB_t25898	-	tRNA-Thr	n.a.
	PVLB_23915	-	hypothetical protein	n.a.
	PVLB_23920	-	hypothetical protein	n.a.
	PVLB_23925	-	hypothetical protein	n.a.
	PVLB_23930	-	hypothetical protein	n.a.
	PVLB_23935	-	hypothetical protein	n.a.
	PVLB_23940	-	hypothetical protein (uncharacterized protein conserved in bacteria)	yes
	PVLB_23945	-	hypothetical protein	yes
	PVLB_23950	-	nucleoid DNA-binding protein	yes
	PVLB_23955	-	hypothetical protein	yes
	PVLB_23960	-	tail fiber assembly protein	yes
	PVLB_23965	-	putative tail fiber protein	yes
	PVLB_23970	-	hypothetical protein (DNA-directed RNA polymerase, β subunit)	yes
	PVLB_23975	-	hypothetical protein (uncharacterized homolog of phage Mu protein gp47)	yes
	PVLB_23980	-	hypothetical protein	yes
	PVLB_23985	-	prophage PSPPH06, TP901 family tail tape measure protein	yes
	PVLB_23990	-	hypothetical protein	yes
	PVLB_23995	-	prophage PSPPH06, lysis protein	yes
	PVLB_24000	-	prophage PSPPH06 lysozyme	yes
	PVLB_24005	-	hypothetical protein	no
	PVLB_24010	-	prophage PSPPH06, DksA/TraR family C4-type zinc finger protein	yes
	PVLB_24015	-	tail tube	yes

Table S4 (continued)

Region	Gene locus tag	Sequence name	Description	Hits against virus and prophage database
prophage 5	PVLB_24020	-	prophage PSPPH06 tail sheath protein	yes
	PVLB_24025	-	prophage PSPPH06, virion morphogenesis protein	yes
	PVLB_24030	-	prophage PSPPH06 tail protein	yes
	PVLB_24035	-	prophage PSPPH06 head completion/stabilization protein	yes
	PVLB_24040	-	putative terminase, endonuclease subunit	yes
	PVLB_24045	-	prophage PSPPH06, major capsid protein P2 family	yes
	PVLB_24050	-	scaffold protein	yes
	PVLB_24055	-	hypothetical protein (Mu-like prophage FluMu protein gp28)	yes
	PVLB_24060	-	PBSX family phage portal protein	yes
	PVLB_24065	-	phage transcriptional activator Ogr/delta	yes
	PVLB_24070	-	hypothetical protein	no
	PVLB_24075	-	XRE family transcriptional regulator	yes
	PVLB_24080	-	hypothetical protein	no
	PVLB_24085	-	hypothetical protein	yes
	PVLB_24090	-	hypothetical protein	no
	PVLB_24095	-	hypothetical protein	no
	PVLB_24100	-	hypothetical protein	yes
	PVLB_24105	-	hypothetical protein	no
	PVLB_24110	-	hypothetical protein	no
	PVLB_24115	-	single-stranded DNA binding protein	yes
	PVLB_24120	-	hypothetical protein	no
	PVLB_24125	-	hypothetical protein	no
	PVLB_24130	-	prophage PSPPH06, site-specific recombinase phage integrase	yes
	-	*attR*	right attachment site (5299872-5299921 bp)	no
	-	*attL*	left attachment site (5299911-5298604 bp)	no
	-	*attL*	left attachment site (5301942-5301953 bp)	no
	PVLB_24140	-	hypothetical protein	no
	PVLB_24145	-	hypothetical protein	no
	PVLB_24150	-	integrase family protein	no
	PVLB_24155	-	phage integrase	no
	PVLB_24160	-	hypothetical protein	n.a.
	PVLB_24165	-	ISPsy20, transposase IstB	n.a.
	PVLB_24170	-	ISPsy20, transposase IstA	n.a.
	PVLB_24175	-	lipoprotein	n.a.
	PVLB_24180	-	hypothetical protein	n.a.
	PVLB_24185	-	hypothetical protein (predicted transcriptional regulator)	n.a.
	PVLB_24190	-	IS4, transposase	
	PVLB_24195	-	ISPs1, transposase OrfA	n.a.
	PVLB_24200	-	stability cassette protein (cytotoxic translational repressor of toxin-antitoxin stability system)	n.a.
	PVLB_24205	-	bifunctional antitoxin/transcriptional repressor RelB (DNA-damage-inducible protein J)	n.a.
	-	*attR*	right attachment site (5312918-5312929 bp)	no
	-	*attR*	right attachment site (5314593-5314665 bp)	no

Abbreviations: n.a., not available.

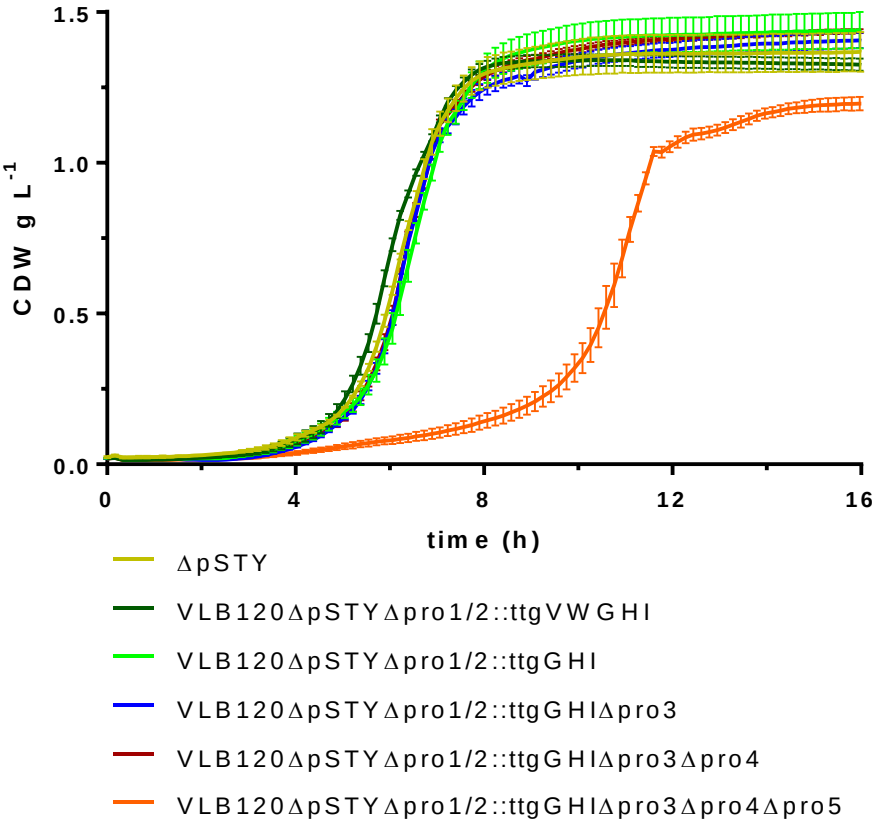

Figure S3. Growth of prophage deletion strains. Growth of the strains harboring genetic deletions of proviral sequences on MSM with 20 mM glucose as sole carbon source. Growth kinetics were measured as backscattered light using the CGQ. The backscatter was converted into CDW according to the biomass yields obtained for the respective cultures. The data for VLB120ΔpSTY is taken from Fig. 5 of the main article and serves as a reference for the tested strains.

Table S5. Biomass yield coefficients of prophage deletion strains. Biomass yield coefficients for the strains resulting from the deletion of proviral segments are shown. The data for the reference strain VLB120ΔpSTY is taken from Table 2 of the main article. The strains were grown in mineral salt medium (MSM) supplemented with 20 mM glucose. The errors are given as standard error of the mean.

***P. taiwanensis* VLB120 strain**	**Biomass yield coefficient $Y_{X/S}$ ($g_{cdw}\ g_{glucose}^{-1}$)**
ΔpSTY	0.377 ± 0.010
ΔpSTYΔpro1/2::*ttgVWGHI*	0.363 ± 0.006
ΔpSTYΔpro1/2::*ttgGHI*	0.401 ± 0.017
ΔpSTYΔpro1/2::*ttgGHI*Δpro3	0.392 ± 0.008
ΔpSTYΔpro1/2::*ttgGHI*Δpro3Δpro4	0.400 ± 0.002
ΔpSTYΔpro1/2::*ttgGHI*Δpro3Δpro4Δpro5	0.330 ± 0.006

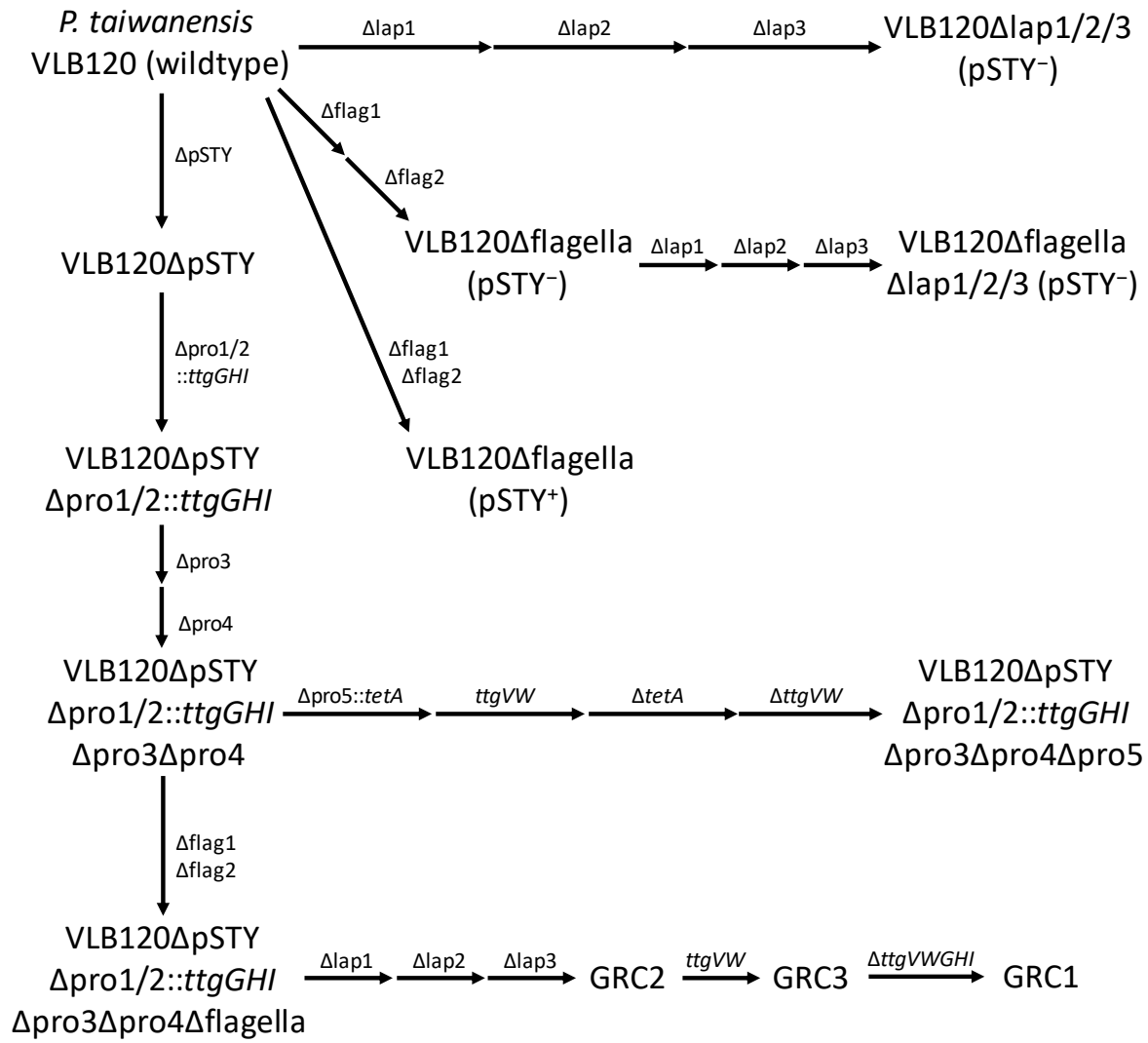

Figure S4. Streamlined chassis strain genealogy. This genealogical tree illustrates the progression and relationship between the generated chassis strains. Each arrow indicates a single deletion procedure.

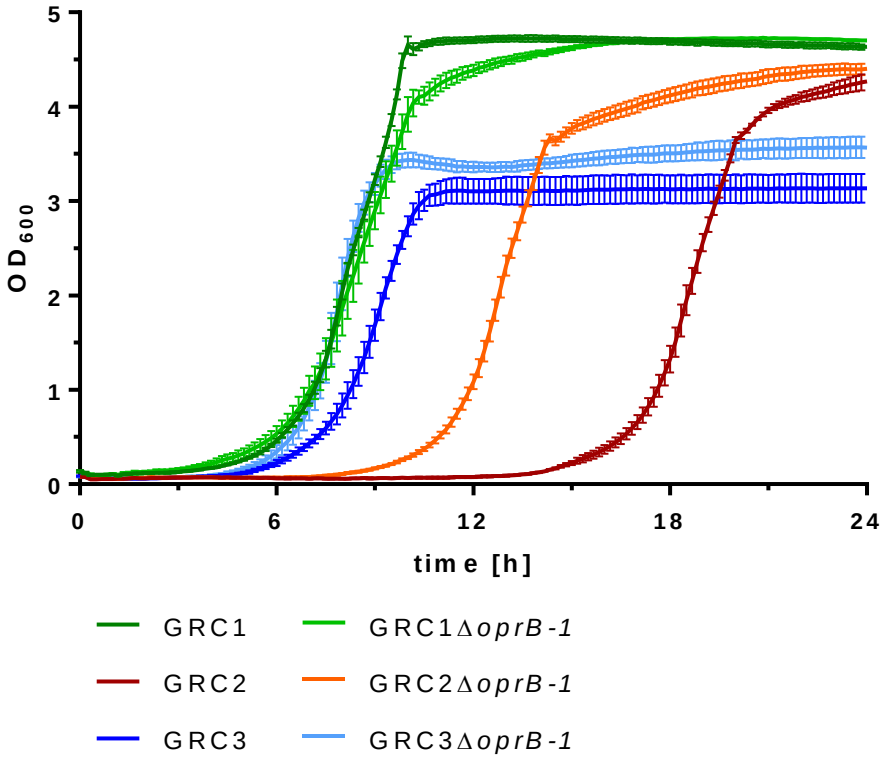

Figure S5. *oprB-1* mutants grown in the presence of phenol. Growth of *P. taiwanensis* GRC1, GRC2, GRC3, GRC1Δ*oprB-1*, GRC2Δ*oprB-1*, and GRC3Δ*oprB-1* in MSM with 20 mM glucose and 5 mM phenol without prior adaptation. Growth kinetics obtained by the CGQ with online scattered light measurement converted into OD_{600} using a calibration**.** Error bars indicate the standard error of the mean (n = 3). The growth curves of GRC1, GRC2, and GRC3 were taken from the main article (Fig. 8) and serve as control.

Table S6. Oligonucleotides. The following oligonucleotides were used as PCR primers in the course of cloning procedures. Shown are their respective designations, sequence, and description. Lower case letters indicate overhangs, letters representing the binding sequence are capitalized, and used restriction sites are underlined. Oligonucleotides used for diagnostic PCRs and sequencing reactions are not included.

designation	Sequence (5' → 3')	description
BW017	agggataacagggtaatctgaattCGAACAGGTTTCCAGGCAACG	TS1-*ppc* forward primer
BW018	ggccatctagaGGTCTGCAAGCGGCCGTC	TS1-*ppc* reverse primer
BW019	cttgcagacctctagaTGGCCCTCTCTTTGGCGC	TS2-*ppc* forward primer
BW020	gaagcttgcatgcctgcaggtcgaCCGCGGACTGGGTGACGG	TS2-*ppc* reverse primer
BW081	gtaatctgaattcgagctcGCCGCCCATTGCCCCAGG	TS1-flag1 forward primer
BW082	accctctagaTCATGATTGTATACAACCTGTCGAACCCG	TS1-flag1 reverse primer
BW083	caatcatgatctagaGGGTTGAGCTTCCCTTAC	TS2-flag1 forward primer
BW084	agcttgcatgcctgcaggtcgacGTCGAAGCGGTCAACAAC	TS2-flag1 reverse primer
BW088	gtaatctgaattcgagctcGACTCGTGAATTGCCTGAAGACAGC	TS1-flag2 forward primer
BW089	gcaatctagaTCAAGCCCGCCGCCTGCT	TS1-flag2 reverse primer
BW090	cgggcttgatctagaTTGCTCGCCTCCTCCGCG	TS2-flag2 forward primer
BW091	agcttgcatgcctgcaggtcgacGGCTCGCCGCTGTCGGCG	TS2-flag2 reverse primer
BW124	ggataacagggtaatctgaattcTGGAAATCTCGACAGCATCG	TS1-pSTY forward primer
BW125	ccaaacccctctagaGACGTTCCAGGCTCCAGG	TS1-pSTY reverse primer
BW131	agcgagttaattaaCTACTGCTGACAGTACTCTGTT	*ttgVWGHI* reverse primer
BW132	taagttggcgcgccCAATATTTGAAATCTAGGGCAG	*ttg(VW)GHI* forward primer
BW133	agggataacagggtaatctgaattcTACGACCAGGGCTTCACC	TS1-prophage1/2 forward primer
BW134	cgcggggcgcgccGGAAAAAAGGCGAAGTCACTC	TS1-prophage1/2 reverse primer
BW135	ccttttttccggcgcgccccgcggttaattaaACCGCCACCCATGACG GG	TS2-prophage1/2 forward primer
BW136	tgcatgcctgcaggtcgactctagaGCGGTTTCGCTCAAGACCTTG	TS2-prophage1/2 reverse primer
BW182	agcgagttaattaaATCTCTCCTCGGCGTGCA	*ttgGHI* reverse primer
BW203	gtaatctgaattcgagctcCAGCTTGAATACCAGCTTG	TS1-*fliL* forward primer
BW204	cggattattggcCGTATTGCAGTAGGAGTC	TS1-*fliL* reverse primer
BW205	tgcaatacgGCCAATAATCCGTCGTCCATCAGGGTTTC	TS2-*fliL* forward primer
BW206	catgcctgcaggtcgactctagaCGTGGCCAGGGTGGCGCT	TS2-*fliL* reverse primer
BW270	ggataacagggtaatctgaattcACGATTATGTCGCCAGAAC	TS1-prophage3 forward primer
BW271	tttgggggagagctcTATGTATGTATACATACATATAGCTTCG	TS1-prophage3 reverse primer

Table S6 (continued)

designation	Sequence (5' → 3')	description
BW272	tacatacatagagctcTCCCCCAAAATTCCCCCA	TS2-prophage3 forward primer
BW273	catgcctgcaggtcgactctagaTCAACGCCTTCATCATGC	TS2-prophage3 reverse primer
BW276	ggataacagggtaatctgaattcAGCACCTCTTCGGTGAAGC	TS1-prophage4 forward primer
BW277	CtgaacgctgagctcGGGCGTTCCTCGCAGTGG	TS1-prophage4 reverse primer
BW278	ggaacgcccgagctcAGCGTTCAGGGGCAGCTT	TS2-prophage4 forward primer
BW279	catgcctgcaggtcgactctagaTAACCGAAAGTCTTCACCACCAG	TS2-prophage4 reverse primer
BW281	gtaatctgaattcgagctcCACAAGCTGTTCTTCAAC	TS1-prophage5 forward primer
BW282	cacaggggcgcgccGAAAGGTTTTTCAGGCTG	TS1-prophage5 reverse primer
BW283	aaacctttcggcgcgccCCTGTGTTCTCCTGCTCA	TS2-prophage5 forward primer
BW284	agcttgcatgcctgcaggtcgacCAATCACTTCAACCAATTCG	TS2-prophage5 reverse primer
BW317	cagcctgaaaaacctttcggcgcgccTTGACAGCTTATCATCGATAAA CTGTAATG	*tetA* forward primer
BW318	tgagcaggagaacacaggggcgcgccTCTCAGGTCGAGGTGGCC	*tetA* reverse primer
BW338	tctgaattcgagctcggtacccgggTTGTACAGTGCCATGTGG	TS1-lap1 forward primer
BW339	agcgcggcgcgccGACGGTTTTAAGTATCCAGG	TS1-lap1 reverse primer
BW340	taaaaccgtcggcgcgccGCGCTGTGCAAGCGTCGG	TS2-lap1 forward primer
BW341	gaagcttgcatgcctgcaggtcgacGCGCGAAGCCGTTCCACC	TS2-lap1 reverse primer
BW346	tctgaattcgagctcggtacccgggGCTGCTGCCGATCATGGT	TS1-lap2 forward primer
BW347	gcgacggcgcgccATGACTGGCGTGGTCGGA	TS1-lap2 reverse primer
BW348	cgccagtcatggcgcgccGTCGCCCGCAGGCCGGCT	TS2-lap2 forward primer
BW349	gaagcttgcatgcctgcaggtcgacGGTTGGTCTTCATATCGGACTCA CGGACCAATGC	TS2-lap2 reverse primer
BW450	gaagcttgcatgcctgcaggtcgacTTGACCGTGCAGGCCAAG	TS1-lap3 forward primer
BW451	gctgaatatagctagcTCAAAGGCCGAGGTACCG	TS1-lap3 reverse primer
BW452	cggcctttgagctagcTATATTCAGCGACAATCTCCC	TS2-lap3 forward primer
BW453	gggtaatctgaattcgagctcGGATGTGCGGGTTGATCTC	TS2-lap3 reverse primer

Table S7. Plasmids. All plasmids used in this study are listed below with relevant characteristics, references, and, if cloned during this work, a brief description of their assembly.

plasmid	relevant characteristics/description	assembly description	Reference
pRK2013	Km^R, *oriV*(RK2/ColE1), mob^+ tra^+		Figurski and Helinski (1979)
pSW-2	Gm^R, *oriV*(RK2), mob^+, *xylS*, $P_m \rightarrow$ *I-sceI*		Martínez-García and de Lorenzo (2011)
pTNS1	Ap^R, *oriV*(R6K), mob^+, TnsABC+D operon for specific transposition		Choi et al. (2005)
pBG42	Km^R, Gm^R, *oriV*(R6K), *Tn7L* and *Tn7R* extremes, P_{14g}-BCD2 → *msfgfp*		Zobel et al. (2015)
pEMG	Km^R, *oriV*(R6K), mob^+, *lacZα*-MCS flanked by two I-SceI sites		Martínez-García and de Lorenzo (2011)
pEMGu	pEMG-derivative with $P_{em7} \rightarrow$ *uidA*	HiFi DNA assembly; *uidA* was amplified from gDNA of *E. coli* K-12 MG1655 and integrated into pEMG via BstBI	Wynands, B. (unpublished)
pEMGg	pEMG-derivative with $P_{14f} \rightarrow$ *msfgfp*	HiFi DNA assembly; *msfgfp* was amplified from pBG42 and integrated into pEMG via BstBI	Wynands, B. (unpublished)
pSEVA412S	Sm/Sp^R, *oriV*(R6K), mob^+, *lacZα*-MCS flanked by two I-SceI sites		Víctor de Lorenzo lab collection
pSEVA512S	Tc^R, *oriV*(R6K), mob^+, *lacZα*-MCS flanked by two I-SceI sites		Víctor de Lorenzo lab collection
pEMGu-*fliL*	pEMGu bearing flanking sequences of *fliL*, *fliL* deletion delivery vector	HiFi DNA assembly; TS1-*fliL* and TS2-*fliL* were amplified from *P. taiwanensis* VLB120 gDNA and integrated into pEMGu via SacI/XbaI	this study
pEMG-flag1	pEMG bearing flanking sequences of the flag1 region, flag1 deletion delivery vector	standard restriction-ligation; TS1-flag1 and TS2-flag1 were amplified from *P. taiwanensis* VLB120 gDNA, fused through splicing by overlap extension PCR and subcloned into pJET1.2/blunt, thereafter TS1-TS2 fragment was restricted and integrated into pEMG via SacI/SalI	this study
pEMG-flag2	pEMG bearing flanking sequences of the flag2 region, flag2 deletion delivery vector	standard restriction-ligation; TS1-flag2 and TS2-flag2 were amplified from *P. taiwanensis* VLB120 gDNA, fused through splicing by overlap extension PCR and subcloned into pJET1.2/blunt, thereafter TS1-TS2 fragment was excised and integrated into pEMG via SacI/SalI	this study
pSEVA512S-flag2	pSEVA512S bearing flanking sequences of the flag2 region, flag2 deletion delivery vector	standard restriction-ligation; the TS1-TS2 fragment was excised from pEMG-flag2 and integrated into pSEVA512S via SacI/HindIII	this study
pEMG-pSTY	pEMG bearing a 500 bp upstream target sequence of the pSTY-located genes *stySRABC*, pSTY deletion delivery vector	standard restriction-ligation; the target sequence was amplified from *P. taiwanensis* VLB120 gDNA and integrated into pEMG via XbaI/EcoRI	this study

Table S7 (continued)

plasmid	relevant characteristics/description	assembly description	Reference
pEMG-pro1/2	pEMG bearing flanking sequences of prophage 1/2 with AscI and PacI restriction site between TS1 and TS2, prophage 1/2 deletion delivery vector	HiFi DNA assembly; TS1-prophage1/2 and TS2-prophage1/2 were amplified from *P. taiwanensis* VLB120 gDNA and integrated into pEMG via EcoRI/XbaI	this study
pEMG-pro1/2-*ttgVWGHI*	pEMG bearing flanking sequences of prophage 1/2 with *ttgVW* and *TtgGHI* between TS1 and TS2, prophage 1/2 deletion delivery and *ttgVWGHI* integration vector	standard restriction-ligation; the *ttgVWGHI* fragment was amplified from the pSTY megaplasmid and integrated into pEMG-prophage1/2 via AscI/PacI	this study
pEMG-pro1/2-*ttgGHI*	pEMG bearing flanking sequences of prophage 1/2 with *ttgGHI* between TS1 and TS2, prophage 1/2 deletion delivery and *ttgGHI* integration vector	standard restriction-ligation; the *ttgGHI* fragment was amplified from the pSTY megaplasmid and integrated into pEMG-prophage1/2 via AscI/PacI	this study
pEMGu-pro3	pEMG bearing flanking sequences of prophage 3, prophage 3 deletion delivery vector	HiFi DNA assembly; TS1-prophage3 and TS2-prophage3 were amplified from *P. taiwanensis* VLB120 gDNA and integrated into pEMGu via EcoRI/XbaI	this study
pEMGu-pro4	pEMG bearing flanking sequences of prophage 4, prophage 4 deletion delivery vector	HiFi DNA assembly; TS1-prophage4 and TS2-prophage4 were amplified from *P. taiwanensis* VLB120 gDNA and integrated into pEMGu via EcoRI/XbaI	this study
pEMGu-pro5	pEMG bearing flanking sequences of prophage 5 with a AscI restriction site between TS1 and TS2, prophage 5 deletion delivery vector	HiFi DNA assembly; TS1-prophage4 and TS2-prophage4 were amplified from *P. taiwanensis* VLB120 gDNA and integrated into pEMGu via SacI/SalI	this study
pEMGu-pro5-*tetA*	pEMG bearing flanking sequences of prophage 5 with a Tc^R marker between TS1 and TS2 , prophage 5 deletion delivery vector	HiFi DNA assembly; the tetracycline resistance marker *tetA* was amplified with its promoter from pSEVA512S and integrated into pEMGu-prophage5 via AscI	this study
pEMGg-lap1	pEMGg bearing flanking sequences of the lap1 region, lap1 deletion delivery vector	HiFi DNA assembly; TS1-lap1 and TS2-lap1 were amplified from *P. taiwanensis* VLB120 gDNA and integrated into pEMGg via XmaI/SalI	this study
pEMGg-lap2	pEMGg bearing flanking sequences of the lap2 region, lap2 deletion delivery vector	HiFi DNA assembly; TS1-lap2 and TS2-lap2 were amplified from *P. taiwanensis* VLB120 gDNA and integrated into pEMGg via XmaI/SalI	this study
pSEVA512S-lap2	pSEVA512S bearing flanking sequences of the lap2 region, lap2 deletion delivery vector	standard restriction-ligation; the TS1-TS2 fragment was excised from pEMG-lap2 and integrated into pSEVA512S via SalI/SacI	this study
pSEVA412S-lap3	pSEVA412S bearing flanking sequences of the lap3 region, lap3 deletion delivery vector	HiFi DNA assembly; TS1-lap3 and TS2-lap3 were amplified from *P. taiwanensis* VLB120 gDNA and integrated into pSEVA412S via SalI/SacI	this study
pEMGu-*oprB-1*	pEMGu bearing flanking sequences of *oprB-1*, *oprB-1* deletion delivery vector		Wynands et al. (2018)

Table S7 (continued)

plasmid	relevant characteristics/description	assembly description	Reference
pEMG-*pobA*	pEMG bearing flanking sequences of *pobA*, *pobA* deletion delivery vector		Wynands et al. (2018)
pEMG-*hpd*	pEMG bearing flanking sequences of *hpd*, *hpd* deletion delivery vector		Wynands et al. (2018)
pEMG-*quiC*	pEMG bearing flanking sequences of *quiC*, *quiC* deletion delivery vector		Wynands et al. (2018)
pEMG-*quiC1*	pEMG bearing flanking sequences of *quiC1*, *quiC1* deletion delivery vector		Wynands et al. (2018)
pEMGu-PVLB_13075	pEMGu bearing flanking sequences of *quiC2*, *quiC2* deletion delivery vector		Wynands et al. (2018)
pSEVA412S-*quiC1*	pSEVA412S bearing flanking sequences of *quiC1*, *quiC1* deletion delivery vector	standard restriction-ligation; the TS1-TS2 fragment was excised from pEMG-*quiC1* and integrated into pSEVA412S via SalI/SacI	this study
pSEVA512S-*hpd*	pSEVA512S bearing flanking sequences of *hpd*, *hpd* deletion delivery vector	standard restriction-ligation; the TS1-TS2 fragment was excised from pEMG-*hpd* and integrated into pSEVA512S via EcoRI/SalI	this study
pEMGu-*trpE*^{P290S}	pEMGu bearing flanking sequences of *trpE*^{P290S}, P290S substitution delivery vector		Wynands et al. (2018)
pEMGg-*aroF-1*^{P148L}	pEMGg bearing flanking sequences of *aroF-1*^{P148L}, P148L substitution delivery vector		Wynands et al. (2018)
pEMGg-*pheA*^{T310I}	pEMGg bearing flanking sequences of *pheA*^{T310I}, T310I substitution delivery vector		Wynands et al. (2018)
pEMG-*pykA*	pEMG bearing flanking sequences of *pykA*, *pykA* deletion delivery vector		Wynands et al. (2018)
pEMG-*ppc*	pEMG bearing flanking sequences of *ppc*, *ppc* deletion delivery vector	HiFi DNA assembly; TS1-*ppc* and TS2-*ppc* were amplified from VLB120 gDNA and integrated into pEMG via EcoRI/SalI	this study
pBG42-*PaTPL2*-*aroG*^{fbr}-*tyrA*^{fbr}	pBG42 with P_{14g} → *PaTPL2*, *aroG*^{D146N}, and *tyrA*^{A354V,M53I}		Wynands et al. (2018)

References

Arndt, D., Grant, J. R., Marcu, A., Sajed, T., Pon, A., Liang, Y., Wishart, D. S., 2016. PHASTER: a better, faster version of the PHAST phage search tool. Nucleic Acids Res. 44, W16-21.

Choi, K.-H., Gaynor, J. B., White, K. G., Lopez, C., Bosio, C. M., Karkhoff-Schweizer, R. R., Schweizer, H. P., 2005. A Tn7-based broad-range bacterial cloning and expression system. Nat. Meth. 2, 443-448.

Figurski, D. H., Helinski, D. R., 1979. Replication of an origin-containing derivative of plasmid RK2 dependent on a plasmid function provided in *trans*. Proc. Natl. Acad. Sci. U.S.A. 76, 1648-1652.

Martínez-García, E., de Lorenzo, V., 2011. Engineering multiple genomic deletions in Gram-negative bacteria: analysis of the multi-resistant antibiotic profile of *Pseudomonas putida* KT2440. Environ. Microbiol. 13, 2702-2716.

Wynands, B., Lenzen, C., Otto, M., Koch, F., Blank, L. M., Wierckx, N., 2018. Metabolic engineering of *Pseudomonas taiwanensis* VLB120 with minimal genomic modifications for high-yield phenol production. Metab. Eng. 47, 121-133.

Zobel, S., Benedetti, I., Eisenbach, L., de Lorenzo, V., Wierckx, N., Blank, L. M., 2015. Tn7-based device for calibrated heterologous gene expression in *Pseudomonas putida*. ACS Synth. Biol. 4, 1341-1351.